Applications in Energy and Combustion Science 27 (2026) 100525

Contents lists available at ScienceDirect

Applications in Energy and Combustion Science

journal homepage: www.sciencedirect.com/journal/applications-in-energy-and-combustion-science

AI assessment of structural fuel load and fire risk via street house images in wildland-urban interface

Yifei Ding [a,b], Thomas Gernay [b,*], Xuechun Li [b], Negar Elhami-Khorasani [c], Susu Xu [b], Xinyan Huang [a,e,*]

[a] Research Centre for Smart Urban Resilience and Firefighting, Department of Building Environment and Energy Engineering, The Hong Kong Polytechnic University, Hong Kong
[b] Department of Civil and Systems Engineering, Johns Hopkins University, Baltimore, MD, USA
[c] Department of Civil, Structural and Environmental Engineering, University at Buffalo, Buffalo, NY, USA
[e] Research Institute for Sustainable Urban Development, The Hong Kong Polytechnic University, Hong Kong

ARTICLE INFO

Keywords:
WUI fire
Residential fire load
Risk assessment
Deep learning
Remote sensing
California wildfire

ABSTRACT

Wildfires directly threaten human lives and properties in the wildland-urban interface (WUI). Combustible materials of house structure are easily ignited by sustained thermal radiation or fire spotting, so the estimation of structural fuel load is critical for accurate WUI fire spread modelling and risk assessment. This work presents a proof-of-concept framework for evaluating structural fuel load that integrates deep learning, remote sensing, and geographic datasets (house images of Google Street View and OpenStreetMap). A convolutional neural network (CNN) model was developed to automatically identify from images the construction materials (e.g., wood, vinyl, metal, concrete, brick) for the exterior walls and roof of residential structures. Remote sensing data was employed to estimate structural dimensions and structural fuel load via combining material properties of density, combustibility, and heat of combustion. The CNN model was trained and validated using real-world data of more than 6,000 structure-material pairs from the 2025 Palisades fire in California, sourced from the CAL FIRE Damage Inspection (DINS) database. The recognition accuracy of structure attributes exceeds 0.7. Additionally, a case study of the 2025 Eaton fire in California was implemented, where the AI-enabled fuel load estimations showed methodological and feasibility and consistency with those derived from the DINS database under consistent assumptions. Overall, our approach advances a proof-of-concept approach for pre-fire hazard assessment by efficiently providing approximate fuel load information under simplified assumptions, which is crucial for fire spread modelling, disaster prevention, and fire emergency response in WUI communities.

Introduction

Wildland fires (Fig. 1a) pose huge threats to the lives and properties of human communities in the wildland-urban interface (WUI) area (Fig. 1b), where natural vegetation coexists with residential buildings. In past years (2006-2024), the United States reported an average of 67,855 wildland fires per year, burning an average of 7.18 million acres annually, underscoring the severity of both fire frequency and burned area [1,2]. When a wildfire reaches a community, residential structures in WUI communities may be ignited and destroyed [3], e.g., 4,552 structures were destroyed in a wildfire in 2024 in the United States (Fig. 1c) [4]. The 2025 Southern California Wildfire caused 30 deaths and left over 31 people missing, and over 14,000 structures were destroyed in the surrounding communities and even impacted city neighborhoods [5]. These events reflect not only the increased frequency and intensity of wildfires, but also critical vulnerabilities in the built environment, particularly in WUI communities [6].

Scientific progress in understanding and modeling WUI fire including thermal exposure, structure fire spread, and post-fire damage, significantly lags behind the research on indoor building fires and other hazards, which have been studied for decades [7,8]. Relevant exposure modes that can lead to structure ignition [9] include heat radiation [10], direct flame contact [11], and firebrands [12]. However, the relative contributions of these fire spread mechanisms vary widely among different fire events [13–17]. To reduce structural vulnerability in WUI fires, building codes and material standards have incorporated

* Corresponding authors.
E-mail addresses: tgernay@jhu.edu (T. Gernay), xy.huang@polyu.edu.hk (X. Huang).

https://doi.org/10.1016/j.jaecs.2026.100525
Received 20 November 2025; Received in revised form 5 June 2026; Accepted 5 June 2026
Available online 7 June 2026

ignition-resistant requirements [18–20]. However, there are significant gaps in how these standards are evaluated, often relying on overly simplified testing conditions that fail to represent multi-factor coupling fire risk in the real-world [7].

Post-fire analyses have highlighted that construction materials [21] and the spatial arrangement of combustible components [16] are leading factors in building ignition and loss, alongside other factors including windows, vents, eaves that can provide ignition pathways. The ignition probability and damage level of a structure in the WUI fire are significantly affected by its properties (e.g., construction types and materials of roof, wall, deck, and fence), the weather conditions (e.g., temperature, humidity, wind speed and direction), and the surrounding environment (e.g., vegetations, landform, elevation) [22]. Among them, the structural fuel load (SFL), referring to the amount of fixed combustible materials of a house, forms house fuel load (HFL) with the indoor fuel load (IFL) [23,24], influences the ignition, fire spread, and consequences. The HFL should be quantified as a hazard component representing the potential maximum energy release contributes to the overall WUI fire risk. However, current community-level fire assessments rarely account for structure-specific fuel load, for example resulting from the use of various roof and wall siding materials, and the spatial distribution of structures.

Simulating the response of houses to nearby WUI fires remains in the exploratory phase [26–28], leading to challenges and uncertainties for community stakeholders in conducting risk assessments and developing effective mitigation and response strategies [29]. Masoudvaziri et al. [28] proposed a WUI fire tracing model using distribution maps of structures and vegetations, considering heat radiation and firebrands for ignition [30]. In this model, firebrand generation is based on the experiment statistics and the roof area [31] with a constant total generation time for each combustion cell. Qin et al. [27] introduced a model that uses heat release rate (HRR) as a key parameter of firebrand generation mechanism, but it also assumes a constant HRR for all structural cells. These models lack structural fuel load (SFL) as a variable, overlooking differences in structural types and materials, limiting their applicability. Yet, in real WUI fire events, it is observed that some houses ignite and burn down while others subjected to similar conditions appear to survive undamaged, and factors affecting ignition propensity have been studied in laboratories, for example, by IBHS [32]. Several studies explored the correlation between building construction features (e.g., the presence of vent screens and decks, and exterior wall materials) [16] and the extent of wildfire damage to structures through statistical analysis [21]. However, the house safety forecast in WUI fire is a multivariate problem that requires a comprehensive solution considering multi-factor and highly-nonlinear fire damage mechanisms.

With the development of artificial intelligence (AI) technology, especially deep learning, AI has been widely applied to solve fire engineering problems with multi-factor coupling that physics-based equations cannot resolve, either due to complexity or temporal and spatial resolution and computational time challenges. AI can be leveraged to identify the structure type, materials, and dimensions to estimate the fuel load [33]. Our previous work [34,35] had preliminarily explored automated estimation of indoor fuel load (IFL) and a tunnel with dynamic traffic flow based on images of different fuel types and intelligent computer vision. Compared to indoor fuel contents, quantifying combustible structure members in a scalable way is more challenging due to the complexity of construction and the use of composite materials such as studs and insulation layers, which are relatively harder for AI recognition and require deep exploration.

Moreover, remote sensing technology is applicable for community-scale measurement, which requires using deep learning and computer vision algorithms to process the high-resolution satellite images. Traditional fuel load survey methods such as direct weighing [36], inventory method [37], and questionnaire survey [38] either limit the ability to measure heavy fixed components and consumes much time or over-rely on the investigator's self-judgement. The most reliable quantifying fuel load method is the burning test of a full or reduced-size house to measure how much the heat released totally [39–41], while this kind of test is not applicable to community-scale structural fuel load assessment, but the testing results can be the valuable reference. Overall, AI technology is well-suited to provide a rapid processing solution for individual SFL measurement in a community.

To this end, we propose an AI-based structural fuel load identification method using a multi-source data pipeline integrating (1) inspection records, (2) open-source geospatial data, and (3) automated house images captured via Google Street View, filtered by vision-language models (CLIP). We train convolutional neural networks to classify material types and estimate structural dimensions, which allows calculating combustible surface areas. Then, using heat of combustion values and archetype house construction systems quantities, we compute fuel loads based on identified assemblies, construction materials, and combustible areas. This work aims to improve fire hazard characterization and fuel load input for downstream fire spread and risk models.

Data collection

Fig. 2 shows three data sources used in extracting different key information of structures in WUI houses. The data is taken for 10,463 residential houses located in the areas affected by the 2025 Eaton and Palisades fires, located in Los Angels, California, United States. First, we extract structure attributes, including the categories for siding and roofing, and structure type (e.g., single or multi-story), from the open CAL FIRE Damage Inspection (DINS) Dataset [42]. Second, we utilize remote sensing (RS) data, specifically open Geographic Information System (GIS) sources [43], to extract building footprints corresponding to the house addresses recorded in the DINS. The extracted footprint images are further processed to identify structural dimensions, serving as the input parameters to quantify the material quantity of structural components. Third, batches of house images extracted from Google Street View are used as input to the AI model for recognizing structural attributes. The structure attributes record in the DINS serve as the ground-truth labels for training and validating the AI model used for

Fig. 1. (a) Wildland fire, (b) Community in WUI fire, and (c) Destroyed structure after WUI fire (the images are original from https://www.tasnimnews.com/en, licensed under CC BY 4.0.).

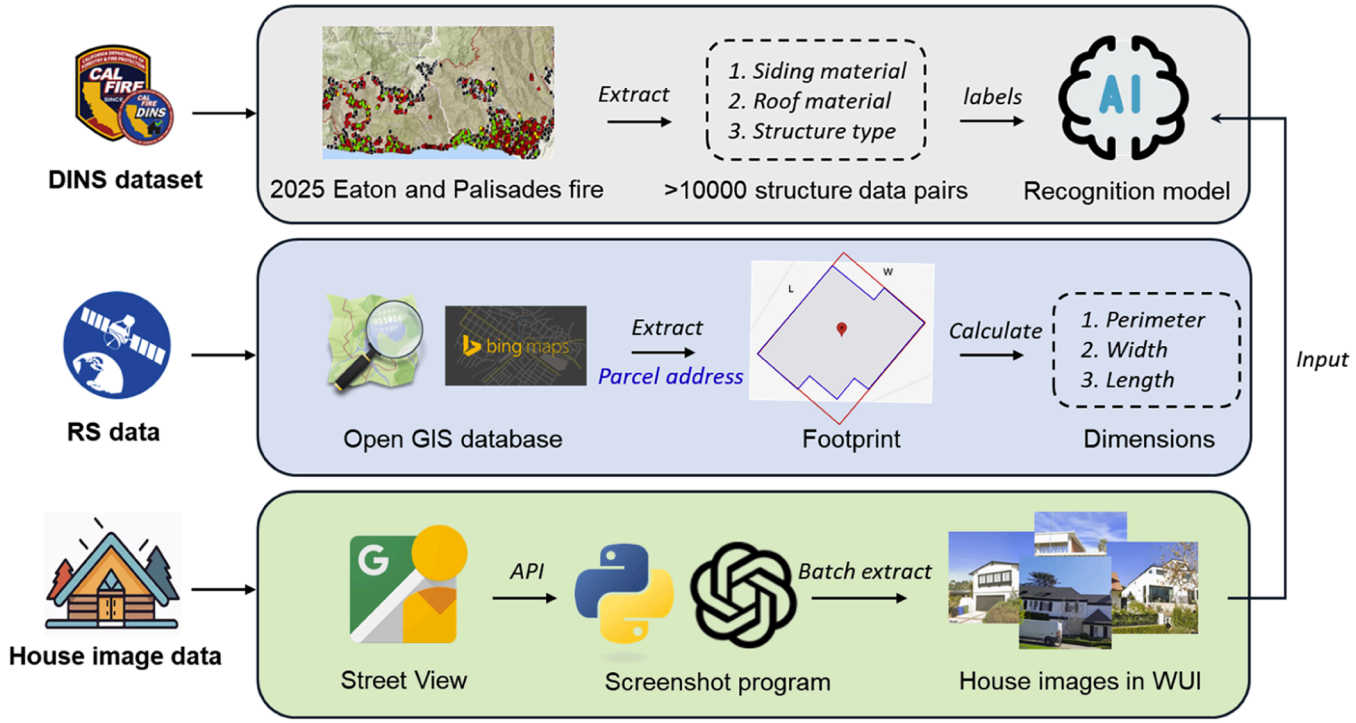

Fig. 2. Data compilation for the AI-based fuel load assessment.

structure recognition from house images.

DINS dataset

The data required for AI model development and validation derives from the 2025 Eaton fire and Palisades fire in Southern California (shown as Fig. 3), which was published by the DINS Dataset [42]. This database includes structures affected by wildland fires located within or up to 100 meters from the fire perimeter. Key details, such as damage degree (No damage, Affected, Minor, Destroyed, etc.), structure type (single family residence single story, single commercial building multi story, etc.), construction features (roof material, exterior wall structure, enclosed eaves, fence attached to structure, etc.), and other relevant features (vent screen, window pane, deck structure), are recorded to the best extent possible, even when the structure is completely damaged.

In this study, the overall methodology aims to estimate structural fuel load by quantifying the amounts of various combustible materials present in structural components specifically, wall and roof (including studs and truss). Accordingly, the relevant information extracted from the DINS database includes parcel address, structural type, materials of roof and exterior wall, as shown in Table 1. The latitude and longitude coordinates are used to support further data retrieval from GIS databases. The structure type classified as either single-story or multi-story is used to approximate the structure height. For single-story structures, the height is assumed to be 3.81 meters (12.5 feet). For multi-story structures, the height is assumed to be 6.55 meters (21.5 feet). The material categories can be matched with corresponding values of effective heat of combustion to approximately determine the amount of energy contained

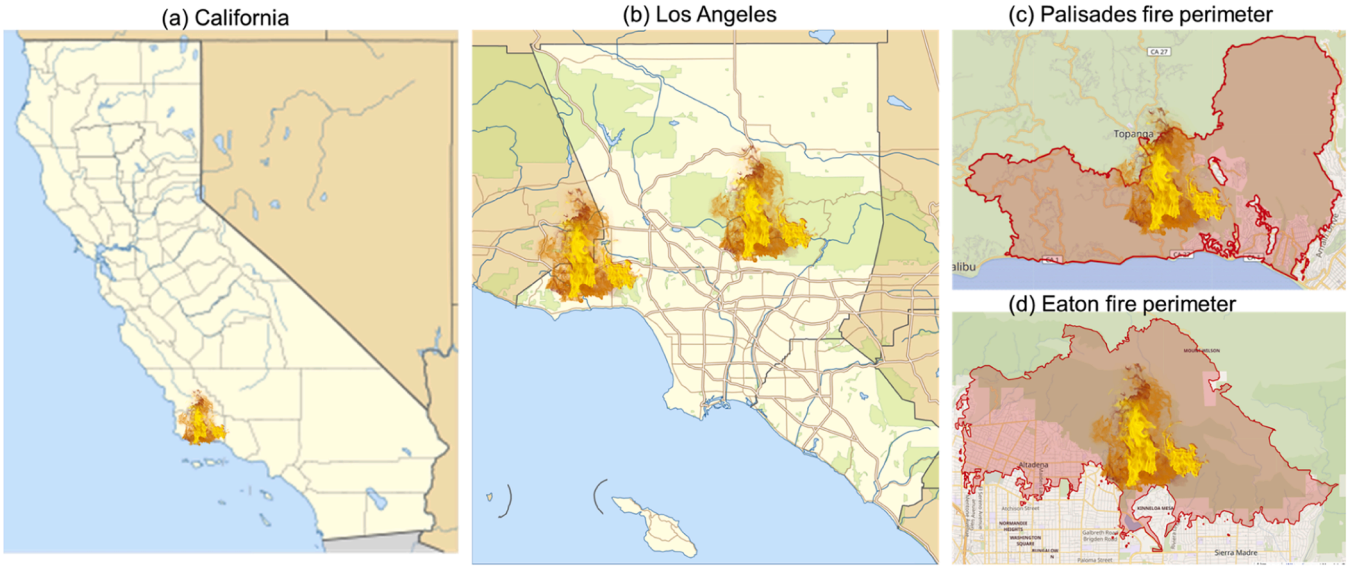

Fig. 3. Location and fire perimeter of study area of 2025 Palisades Fire and Eaton Fire.

Table 1
Data frame extracted from the DINS database.

Location	Purpose	No. of data pairs	Data type
Palisades	AI development	6,392	(1) Address, (2) Roof material, (3) Wall material, and (4) Structure type
Eaton	Case study	4,071	

per unit area in roof and exterior wall, where this process is introduced in detail in Section 3.2. Furthermore, the material information for the roof and exterior wall provided in the DINS database serves as the ground truth for training the AI model in material recognition. Each material label, corresponding to a house image obtained from Street View, forms a data pair used for AI model training.

Therefore, for those communities recorded in the DINS database, structural attributes can be directly obtained from the existing data. However, for communities that are not included in the DINS database or are difficult to retrieve from other open data sources, an AI-based method can then be used to recognize their attributes from their images, where the AI model is developed and trained using data from the DINS dataset. In total, we collected 6,392 data pairs in the Palisades fire and 4,071 data pairs in the Eaton fire, which respectively serve as the data for AI model development and the case study data to validate the proposed method.

Remote sensing data

Remote sensing data is used for acquiring the geometric dimensions of building footprints. The open-source GIS software QGIS Desktop (version 3.40.5) [44] is utilized to extract detailed footprint information from public geospatial datasets GIS sources, e.g. OpenStreetMap [45] and Bing Building Footprints [46]. The data extraction and processing workflow consists of the following four primary stages shown as Fig. 4:

Stage 1: Base map importation. Import the base map layer of the target areas, here the neighborhoods impacted by the Eaton and Palisades in Los Angeles, to provide spatial context and facilitate feature alignment.

Stage 2: Retrieval of building footprints. Retrieve all relevant building structures, especially residential houses, in the target area, and download their footprints from QuickOSM plug-in. This tool allows for efficient extraction of vector footprint data from OpenStreetMap by specifying semantic tags (e.g., *building* = *residential*). The retrieved footprints were stored as an independent polygon layer in the QGIS environment for subsequent processing.

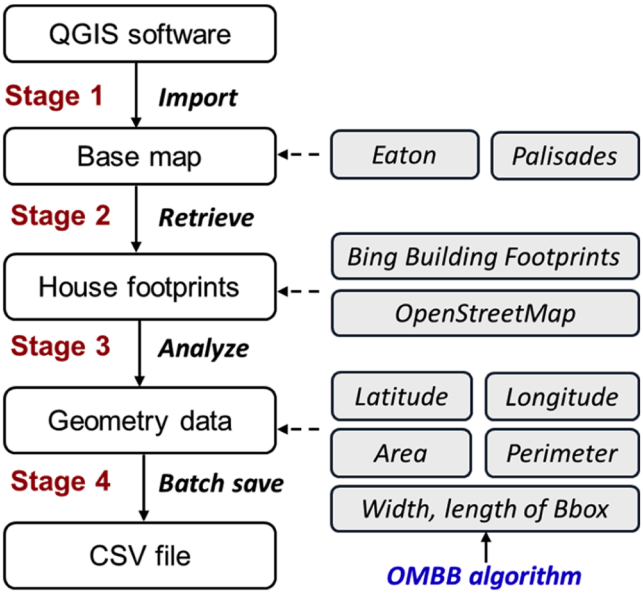

Fig. 4. Flowchart of remote sensing data collections.

Stage 3: Attribute enrichment and geometric analysis. Edit the attribute table of the building footprint layer to include additional parameters such as latitude, longitude, perimeter, width, and length of the bounding box (Bbox). The geographic coordinates (latitude and longitude) were calculated using the centroid of each footprint. In this step, the 2D Oriented Minimum Bounding Box [47] algorithm is used to estimate the width and length of each footprint, especially for irregularly shaped polygons. This method generates the smallest possible rotated rectangle that fully encloses the footprint. The pseudocode of the 2D Oriented Minimum Bounding Box algorithm is shown as Algorithm 1 in Appendix.

Stage 4: Batch export of attribute data. After all required attributes were computed and validated, the enriched building footprint dataset was exported in batch, for integration with structural attributes data and subsequent analysis.

Structure image acquisition by Street View and large language model

An AI model is developed to recognize structural attributes from input house street images (RGB format photo). This allows generalized use of the methodology for wildfire hazard assessment in communities for which an extensive database such as the DINS (which contains structural attributes) is not available. The development of the AI model relies on large datasets of pairs "images-structural attributes" collected for areas covered by the DINS dataset; these are needed for training and validation. Then, the AI model can be used in future applications with other communities provided house images are collected, which is usually more readily available. To this end, we developed an automated image acquisition script based on the API key of Google Street View Map and the Large Language Model. The workflow consists of the following four main steps shown as Fig. 5:

Step 1: Location resolution. To ensure that the program accurately retrieves the structure location in Google Street View, we adopt two location resolution methods: Directly parsing latitude and longitude values, and Geocoding textual addresses using Google Map API. Therefore, the program automatically resolves the input spreadsheet by reading each row and extracting the location columns including "Site address", "Latitude", and "Longitude" for location query.

Step 2: Image retrieval via Google Map API. For each resolved coordinate, the script queries the Google Map API to verify whether panoramic image exists at the target location. Only locations with valid Street View data proceed to the screenshot stage. For these, the program then retrieves multiple images per target location, varying across camera headings (i.e., 0°, 45°, 90°) and fixed pitch angles (10°), with a consistent field of view (40°). This configuration increases the likelihood of capturing building facades from diverse perspectives. Each image is requested at a fixed resolution (1200 × 800 pixels) and stored in memory for subsequent analysis. The copyrights of all images from Google Street Map belong to Google.

Step 3: House recognition using Vison Language Model. In this process, the pre-trained Contrastive Language–Image Pretraining (CLIP) [48] model is used to assist in determining whether the screenshot image contains a valid representation of a "house". CLIP is a multimodal model developed by OpenAI that learns to understand images and natural language together by training on large-scale image–text pairs. The architecture consists of two separate encoders, for image that is Vision Transformer (ViT) and for prompt that is a Transformer-based language model. The output of each encoder network is a 512-dimension embedding semantic vector that represents its meaning or content, called semantic features.

Firstly, each image is transformed into a 512-dimensional feature vector by ViT model in CLIP. At the same time, the pre-written prompt (see Fig. 5), some that describe houses (like "a front view of a house")

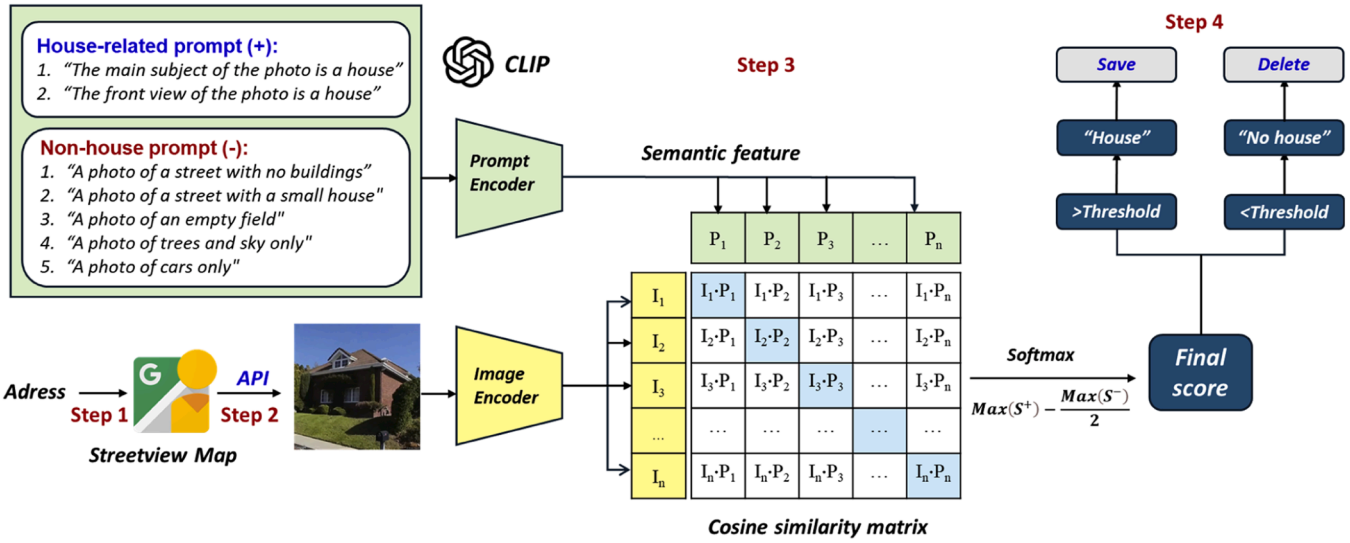

Fig. 5. Flowchart of structure image acquisition by Google Street View and Large Language Model (CLIP).

and some that describe things without houses (like "a photo with no buildings"), are also converted into semantic features. After that, the algorithm compares the image and each text prompt by calculating the Cosine Similarity, shown as Eq. (1), between their semantic vectors. These similarity scores are further turned into percentages using the Softmax function, shown as Eq. (2). To decide if the image shows a house, the final score is computed by Eq. (3), where $Max(S^+)$ is the highest score from the house-related prompts and $Max(S^-)$ is the highest score from the non-house prompts. If the final score is higher than a set threshold (0.5 in this work), the image is considered to contain a house.

$$Cosine\left(\vec{I},\ \vec{P}\right) = \frac{\vec{I}\cdot\vec{P}}{\|\vec{I}\|\cdot\|\vec{P}\|} = \frac{\sum_{i=1}^{512}\left(\vec{I}_i \times \vec{P}_i\right)}{\sqrt{\sum_{i=1}^{512}\vec{I}_i^{\,2}} \times \sqrt{\sum_{i=1}^{512}\vec{P}_i^{\,2}}} \tag{1}$$

$$s(c_j) = \frac{e^{c_j}}{\sum e^{c_j}} \tag{2}$$

$$k = Max(S^+) - Max(S^-)/2 \tag{3}$$

where, $\vec{I}$ and $\vec{P}$ respectively represent semantic vector of the screenshot image and the prompt. c_j is the cosine similarity between the image and prompt j, and s is the similarity score in percentage format using Softmax. k is the final score. S^+ and S^- respectively represent the similarity scores from the house-related prompts and the non-house prompts.

Step 4: House image saving. Images deemed to contain houses are retained and stored in the specified directory using a structured filename.

Overall, data preparation in this work contains three categories: 1. the DINS dataset, which provides training and reference data of structural attributes for AI development, 2. remote sensing data, which provides basic dimensions of house footprint, and 3. structural image data, which is input to the AI model for attribute recognition and also serving as part of the AI training dataset. The summary of the above data collection is listed in Table 2.

Table 2
Summary of data preparations.

Source	Original data	Purpose
DINS	Structural attributes	Reference data for AI
Open GIS	Footprints	Footprint dimension
Street View	Structural images	Attribute recognition by AI

Methodology

Images are used to identify the type of wall or roofing, but fuel load quantification requires knowledge of the volume – i.e., the amount and type of materials across the wall or roof section as well. To address this, we define prototype walls and roofs and evaluate their fuel load density (per surface area) based on cross-section assembly, material quantities, and effective heat of combustion of combustible materials. The prototype assumptions (materials, structures, assemblies) are based on the construction handbook and codes [49,50] in the United States. These evaluations are validated through comparison with real-world combustion test data.

Geometry and dimension of house prototype

Considering the complexity and diversity of various housing and building structures crossing different WUI communities, the identification and classifications follow several key assumptions:

- All structures are assumed to be single-family residential buildings, either single or multi-story.
- The roofs of all structures are assumed to follow the Simple Hip style, shown as Fig. 6. The roof pitch, i.e., the steepness, is set as 1:1, corresponding to a roof angle of 45°.
- Ventilation openings, chimneys, eaves, decks, patios, and fences are excluded from the fuel load assessment.
- The structural fuel load in this work refers only to the external structural components, including roof, exterior wall, and corresponding roof truss and wall studs. The combustible items inside the building, such as furniture and electronics are not considered.
- The materials of both the roof truss and wall studs are assumed to be timber.

According to the geometric feature of a typical house, all dimensions of the structure can be represented by four basic inputs: (1) perimeter of the house footprint (P), (2) Height of the house (H), (3) Length of the house footprint (L), and (4) Width of the house footprint (W). The surface area of roof material is calculated as

$$A_{roof} = (L - W + L) \times\ 0.71W \times \frac{1}{2} \times\ 2 + W \times\ 0.71W \times \frac{1}{2} \times\ 2 \tag{4}$$

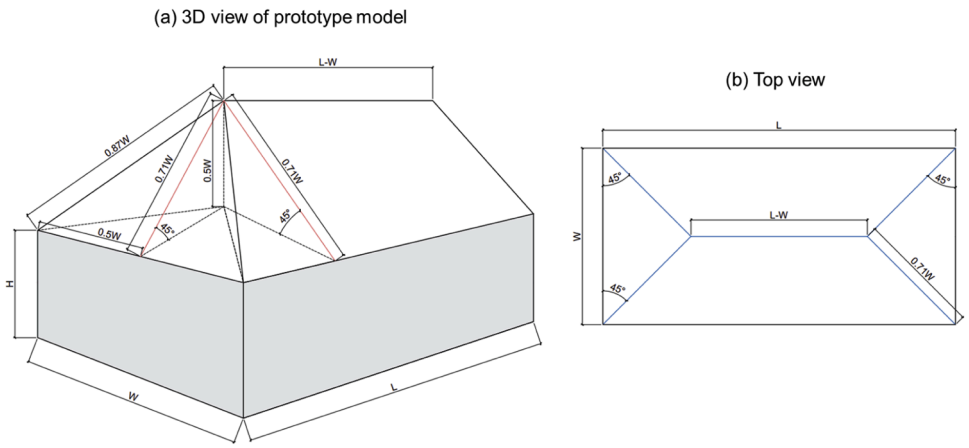

Fig. 6. House prototype for structural fuel load (SFL) assessment, (a) 3D view and (b) top view.

After combining the terms in Eq. (4),

$$A_{roof} = 1.414 \cdot L \cdot W \tag{5}$$

The surface area of the wall material is calculated as

$$A_{wall} = P \cdot H \tag{6}$$

where P represents the footprint perimeter of the structure, obtained from the GIS data.

Fuel load density of structural wall and roof

The construction details of the typical exterior sidewalls of the residential buildings are illustrated in Fig. 7. The principal components from the interior surface to the exterior are the gypsum board (drywall), wood frame, insulation layer, and exterior wall. DINS dataset records four categories of wall siding materials, i.e., wood, vinyl, metal, and stucco/brick/cement. The section dimensions for shingle siding are 6 in × 0.5 in (125 mm × 12.7 mm). An atypical rigid insulation layer is composed of polystyrene with a thickness of 1 inch. The support frame is generally made of wood stud with a cross-section of 2 in × 6 in (50.8 mm × 125 mm), and spaced 24 inches (610 mm) apart. Behind the studs is a 0.5-inch-thick (12.7 mm) gypsum board. Unlike the other three wall types, the wood-sided walls (Fig. 7a) have an extra layer of building paper (154 g/m^2) and a plywood sheathing board with a thickness of 0.5 inch. The fuel load distribution per unit area of each material layer of the wood sidewall is listed in Table 3. The total fuel load of a wood-sided wall is 153.4 MJ/m^2.

Metal (Fig. 7c) and stucco brick cement (Fig. 7d) are considered non-combustible. Even though vinyl (Fig. 7b) has combustible properties under sufficient external heat exposure, their contribution to fire spread and sustained burning is generally considered to be lower compared to

Table 3
Fuel load calculation of wood sidewall construction [51].

Material	Density (kg/m^3)	Volume (m^3/m^2)	Heat of combustion (MJ/kg)	q_{wall_siding} (MJ/m^2)
Wood shingle siding	320	0.0127	12.9	52.4
Building paper (kraft)	/	/	16.4	2.5
Plywood sheathing	500	0.0127	11.1	70.6
Rigid insulation (EPS)	28	0.0254	39.2	27.9
Cavity insulation	/	/	/	/
Gypsum board	/	/	/	/
Total				**153.4**

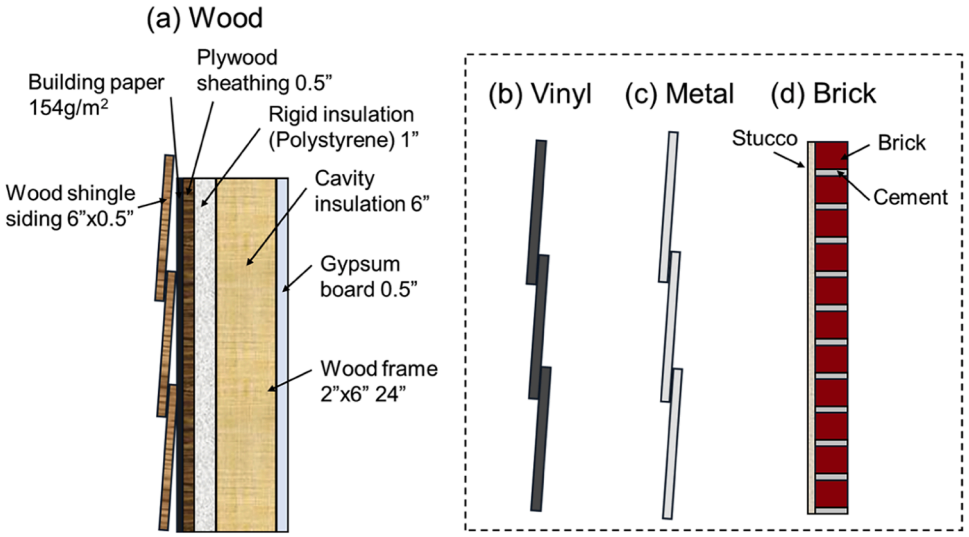

Fig. 7. Construction details of various wall structures.

typical structural fuels such as wood [52]. In this study, vinyl shingles are not included as contributing fuel in the fuel load estimation. This assumption is adopted as a simplification within the proposed framework, which prioritizes materials with more dominant and well-characterized roles in fire growth and spread. It is acknowledged that this treatment may introduce limitations, particularly in scenarios where vinyl materials are exposed to intense heat. Apart from wood sidewall, the combustible components of the other three categories of wall only include the rigid insulation and the wood frames. Therefore, the values of total fuel load per square meter of vinyl, metal, and brick are the same at 27.9 MJ/m^2. Additionally, the wall structures are nailed on wood studs placed 24 inches (610 mm) apart with a fuel load density is 65.7 MJ/m^2.

The construction detail of a typical roof structure with a simple hip style is illustrated in Fig. 8. The roof includes a timber truss and exterior roof siding. The timber truss consists of a rigid board, four hip rafters, four girders, the jack, and common rafters placed 24 inches (610 mm) apart. All truss components have a cross-section of 2 in × 6 in (50.8 mm × 125 mm). The total fuel load of timber truss can be formulated as a function of W and L unit in meters as

$$Q_{truss} = \left(0.007W^2 + 0.018LW + 0.034W + 0.023L\right) \times 355 \times 12.3 \tag{7}$$

where 355 is the density of wood stud unit in kg/m^3, and 12.3 is the value of heat of combustion of wood stud in MJ/kg.

Similar to the wall, the roof structure also includes roof siding with several flammable layers contributing to total fuel load. The main components of roof siding consist of a shingle layer with dimensions of 2 in × 6 in (50.8 mm × 125 mm), a nylon ventilation mat with 4.88 kg per square meter, 30 lb. roofing felt underlayment with a thickness of 1.2 mm, a layer of PVC membrane with a thickness of 0.06 inches, a plywood sheathing with a thickness of 0.625 inches (15.9 mm), and a rigid polystyrene insulation layer with a thickness of 0.75 inches (19.1 mm). The fuel load distribution per unit area for each material layer in the wood roof siding is listed in Table 4. The total fuel load per square meter of wood roof surface is 340.7 MJ/m^2. Other roof covering materials recorded in the DINS dataset, i.e., asphalt, concrete, tile, and metal are considered non-combustible. Therefore, for the roof constructions with these materials the fuel load excludes the shingle layer, whose total fuel load is 288.3 MJ/m^2.

The structural fuel load (SFL) equals the sum of fuel load from the walls and roof, given by:

$$Q_{SFL} = Q_{wall} + Q_{roof} \tag{8}$$

where, the fuel load of wall and roof surface can be formulated as,

$$Q_{wall} = Q_{wall\_siding} + Q_{stud} \tag{9}$$

Table 4
Fuel load calculation of wood roof surface construction [51].

Material	Density (kg/m^3)	Volume (m^3/m^2)	Heat of combustion (MJ/kg)	$q_{roof\_shingle}$ (MJ/m^2)
Wood shingle siding	320	0.0127	12.9	52.4
Nylon ventilation mat	/	/	29.5	144
Roof felt underlayment	699	0.0012	22.8	19.1
PVC membrane	1,388	0.0015	12.8	26.7
Plywood sheathing	500	0.0127	11.1	70.6
Rigid insulation (EPS)	28	0.0254	39.2	27.8
Total				**340.7**

$$Q_{roof} = Q_{roof\_shingel} + Q_{truss} \tag{10}$$

$$Q_{wall\_siding} = A_{wall} \cdot q_{wall\_siding} \tag{11}$$

$$Q_{stud} = A_{wall} \cdot q_{stud} \tag{12}$$

$$Q_{roof\_shingle} = A_{roof} \cdot q_{roof\_shingle} \tag{13}$$

Method validation by fire test

To benchmark the fuel load evaluation of prototype wall and roof assemblies discussed above, we compared computational results with a group of 1/3 scale reduced-size house fire experiments conducted by Himoto et.al [40]. In their tests, 15 wooden model houses were burned to investigate the fire spread among multiple houses, similar to a fire in a WUI community. Each model house had a square footprint of 3.6 m × 3.6 m, with heights ranging from 2.55 m to 3.15 m. The exterior walls were constructed with 12-mm-thick gypsum board, and the roofs were covered with 12-mm-thick cedar plywood, both mounted on timber frameworks. Each house has 16 openings allocated on each wall, and they were left open during combustion tests. In addition, approximately 250 kg of wood crib was placed inside each model house to serve as fuel.

To ensure consistency with the experimental setup, we adopted the same dimensions and materials of roof and wall and opening sizes in our prototype model. We subtracted the heat contribution from the wood crib to isolate the structural fuel load. Since the specific value of heat released in burning wood cribs was not reported in the literature on Himoto's experiment, we referenced experimental data of wood crib fire from other literatures [53,54]. For example, the Fire Calorimetry Database provided by NIST [53] reports a total heat release by burning out a 36.54 kg wood crib is 597 MJ, so the heat of combustion is 16.3

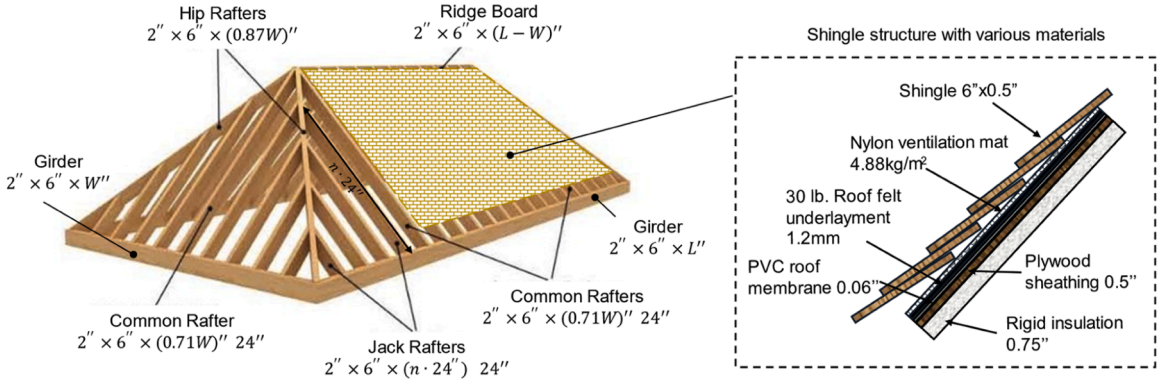

Fig. 8. Construction details of roof timber truss structure assembly.

MJ/kg; and similar values ranging from 15 to 20 MJ/kg were found in different fire calorimetry tests [54]. Based on the NIST values, we estimated that the total fuel load from a 250 kg wood crib is approximately 4,085 MJ. Table 5 lists the measured fuel load values for 15 test houses. The mean value of the total structural fuel load of 15 houses was 7,277 MJ, which reduced to 3,192 MJ after subtracting the heat contribution from the wood crib. The total fuel load of Test D is noticeably lower than that of the other tests, which may be attributed to its location at a corner and the incomplete combustion caused by the wind direction change during the test. The fuel load calculated by our physical model for the same house configuration is 3,056 MJ, resulting in an error of only 4.3%. This comparison demonstrates that our computational method is capable of reliably assessing the potential heat release, i.e., the structural fuel load relevant to fire spread in the WUI community.

AI Method for image recognition by CNN model

We adopt ResNet-50 convolutional neural network (CNN) as the backbone AI model to identify the structure attributes, including roof materials, wall materials, and the structure type (single or multi-story). The ResNet-50 model is a deep convolutional neural network with 50 layers as a part of Residual Network (ResNet) families developed by He et al. [55], which is widely used for computer vision task, such as image classification [56], image feature extraction [57], and object detection [58]. To address the saturation and degradation issues with an increasing number of network layers [59], ResNet allows the network to learn residual functions with reference to the layer inputs, instead of learning unreferenced functions.

Fig. 9 illustrates that the input is a house image, and the output is a 3-dimensional vector including roof material, wall material, and structure type. There are five categories of roof material, four categories of wall material, and two categories of structure type (i.e., single or multi-story). The dataset for model development consists of over 6,000 house images located in Palisades. The images are collected from Google Street View and filtered by CLIP algorithms introduced in Section 2.3. The label of each corresponding image is extracted from the DINS database introduced in Section 2.1. Therefore, the components of one data pair include one image and its label with a 3-dimensional vector.

Batch assessment of structures in a WUI community

In this section, the entire process of batch assessment of structure fuel loads in a WUI community is introduced containing (1) data collection of footprint data and pictures of all structures in the target community, (2) recognition of structure attributes by AI model, (3) fuel load calculations by the physical equations, and (4) fuel load mapping for visualization, respectively introduced in Section 4.1- 4,4.

Table 5
Measured heat release of 15 model houses in Himoto's experiment [40], where the Structural Fuel Load excludes the wood cribs (non-structural indoor fuel).

Test house	Total Fuel Load (MJ)	Structural Fuel Load (MJ)	Ratio of Structural Fuel Load
A	8,366	4,282	51%
C	5,867	1,783	30%
D	4,926	841	17%
E	5,670	1,586	28%
F	6,423	2,338	36%
G	8,617	4,533	53%
H	8,918	4,833	54%
I	10,213	6,129	60%
J	8,149	4,064	50%
K	6,331	2,246	35%
L	8,216	4,132	50%
M	7437	3,352	45%
N	6,962	2,878	41%
O	6,085	2,000	33%
P	6,968	2,884	41%
Mean	**7,277**	**3,192**	**44%**
Calculated by AI method		**3,056**	

Batch data preparation

The initial step to assess the structural fuel load distribution of a target WUI community is to collect geographic data of structures in this area. The flowchart of batch data collection of house footprints and pictures is shown as Fig.10. We find the target community in the public GIS database, i.e., Openstreet and Bing map, and search all residential houses. QGIS software is used to download footprints and information about addresses and the coordinates of these structures. A spreadsheet with address information is used as input file to the automatic Google Street View screenshot program (introduced in Section 2.3) to batch acquire the structure pictures. The program can automatically retrieve, select, and save the required house images using the Google Map API and an LLM-based filter. Then, these images are processed by the ResNet model to analyze the structure type and materials Fig. 10.

The footprint data is used to estimate the dimensions of the structures. The dimensional data includes perimeter and area of footprint, and width and length of minimum bounding box. The details of dimension estimation are introduced in Section 2.2.

Structure attribute classification

In the second step, the pictures of the structures are input to the CNN model to classify the structure attributes, as described in Section 3.4-3.5. The classification results are saved as a spreadsheet file containing five columns, i.e., "Image path", "File name", "Structure type", "Roof material", and "Wall structure". The processing speed of AI-based programming is 136.8 frames per second (FPS) tested in a desktop with the following configuration: NVIDIA GeForce RTX 3060, Gen Intel(R) Core (TM) i7–12700F 2.100 GHz. The program can process around 10,000 house images within two minutes. Therefore, the method can be used to batch recognize the structures in a large-scale region using a common computing source in a short time. After the image recognition, the identified structure type and materials are mapped onto the structure prototypes described in Section 3.1 for further calculations of fuel load.

Fuel load calculation

The identified structural materials are matched with the corresponding fuel load density evaluated for prototype roof shingles and wall types. The fuel load values are calculated following Eqs. (4)-(13). L and W respectively represent the length and width of the minimum bounding box of the footprint and P is the perimeter of the footprint, with those parameters extracted from remote sensing data in Section 4.1. H is the height of the structure, which is determined by the structure type identified in Section 4.2. If the structure type is single story, H equals 3.81m. If the structure type is multi-story, H equals 6.55 m. These procedures allow for calculating the fuel load assigned to each structure in a community.

Fuel load mapping

A geospatial visualization of structure fuel load is generated based on building-level data in the target community. The mapping program first extracts structure data from the input spreadsheet including geographic coordinates (latitude and longitude), total fuel load (MJ), fuel load density (MJ/m^2), structure type, roof material, exterior material, and physical dimensions (width, length, height). The fuel load density in the map refers to the total fuel load divided by the footprint area of the structure. A base map is initialized using the *folium* mapping library. The map is centered at the mean latitude and longitude of all valid data points to ensure optimal framing. Multiple tile layers are added, including OpenStreetMap and CartoDB Positron, allowing users to

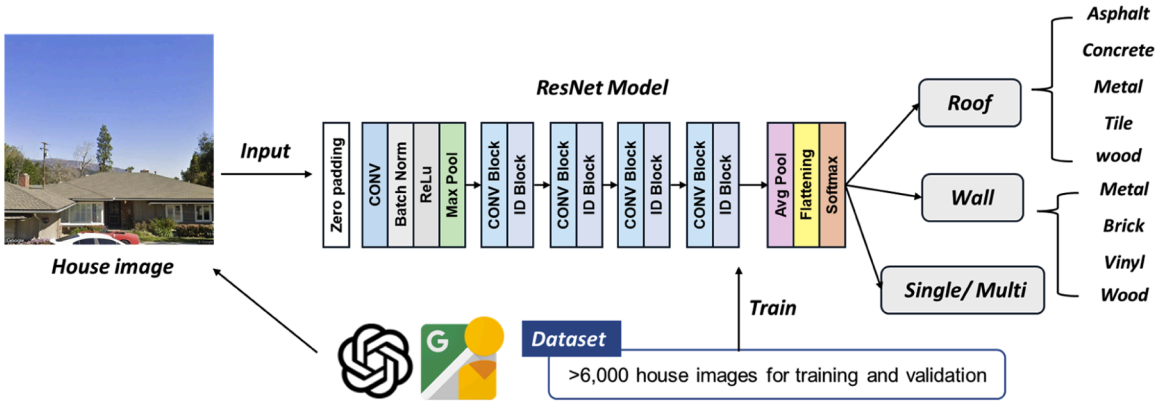

Fig. 9. Architecture of CNN model for structural attribution recognition.

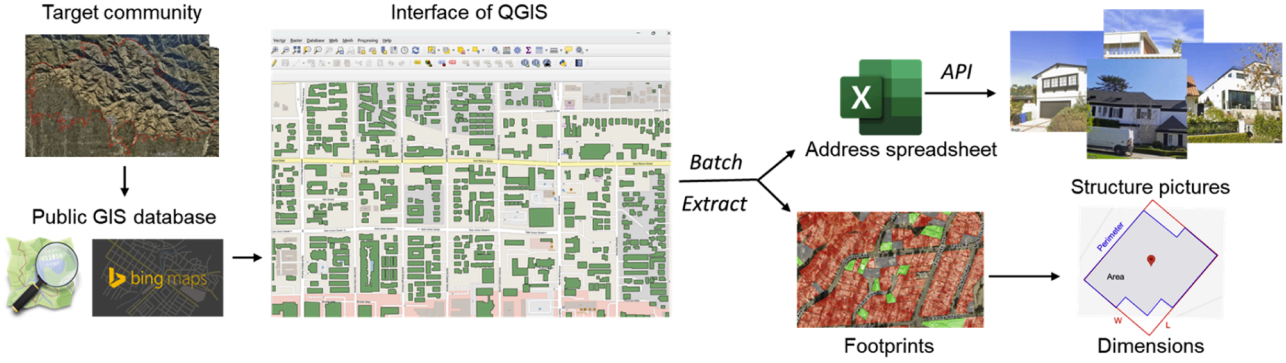

Fig. 10. Flowchart of batch collection of structure footprint data and pictures.

toggle between different basemap styles. The map is configured with a zoom level suitable for local-scale (urban or suburban) visualization, enabling detailed inspection of individual structures.

To visually differentiate buildings based on their potential fire hazard, the total fuel load values are categorized into six discrete intervals: <100, 100–200, 200–300, 300–400, 400–500, and >500 GJ. A custom color scheme is applied to each class using a function that assigns red-hued tones with increasing intensity for higher fuel load classes. This segmentation facilitates rapid visual identification of high-fuel load structures and areas. Each building is represented on the map by a *CircleMarker* plotted at its geographic coordinates. Additionally, each marker is embedded with a popup tooltip that displays detailed structural and fuel information, including total fuel load, density, building dimensions, structural type, and material attributes. To support user interpretation of the color scheme, a custom HTML-based legend is integrated in the bottom-left corner of the map. The structural fuel load map for the communities impacted by the Palisades fire is illustrated in Fig. 11. This legend provides a visual guide to the color coding and its corresponding fuel load intervals. The interactive map is exported and published on https://moric2785.github.io/Structural-Fuel-Load-Map/fuel_load_map.html, and the demonstration of the interactive map is shown as Video S1 in Supplementary Materials. The fuel load map serves as a dynamic input database for researchers concerned with spatial wildfire hazards assessment in the WUI.

Results and demonstrations

The training and testing performance of the recognition model is

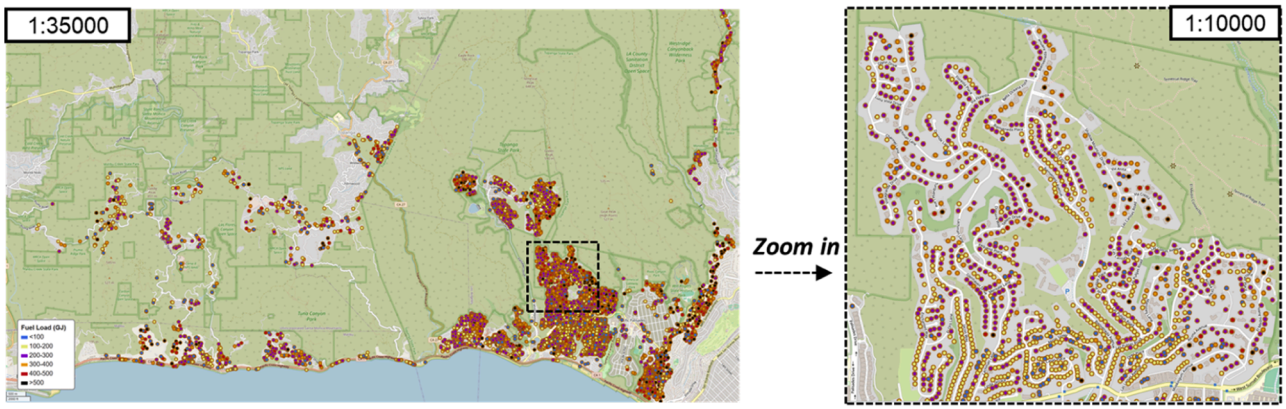

Fig. 11. Structural fuel load map of the community impacted by the Palisades fire with zoom-in details.

introduced in Section 5.1. Additionally, a case study focusing on a community that suffered from the 2025 Eaton fire using our proposed assessment method is demonstrated in Section 4.5-4.6.

AI model training and testing

All labeled data pairs from the Palisades recordings were randomly split into a training dataset and a testing dataset with a ratio of 70% and 30%, respectively. The training dataset is used for training the model, and the test dataset is used to estimate the quality of the fitted model after training. The training process is conducted on a desktop computer with the following configuration: NVIDIA GeForce RTX 3060, Gen Intel (R) Core (TM) i7–12700F 2.100 GHz. Pytorch is applied as the deep learning framework to build the model structure. During training, the batch size is set at 64 and a total of 200 epochs using *AdmaW* (Adam with Weight Decay) optimizer (learning rate of 0.001 and weight decay of 1e-4) are set to make the model fully trained to convergence. To reduce training time and computational resources, the methodology of transfer learning is applied to improve the performance of training results with the limited sample size, so the weight file of the pre-trained ResNet model is loaded as the initial training step.

The loss function in this multi-category classification task adopts Cross Entropy Loss (see Eq. 14) as one of the metrics to evaluate the training performance. Cross Entropy Loss [60] is a commonly used loss function in deep learning classification tasks, which combines Softmax and Log Loss, and is used to measure the difference between the predicted probability distribution and the true class labels. In this work, the CNN model contains three output heads to classify three structural attributes. Therefore, the total loss equals the sum of loss items of each classification as:

$$\mathscr{L} = -\log\left(\frac{e^{zy}}{\sum_{j=1}^{C} e^{zj}}\right) \tag{14}$$

$$\mathscr{L}_{total} = \mathscr{L}_{type} + \mathscr{L}_{roof} + \mathscr{L}_{wall} \tag{15}$$

where, C represents the number of categories, Z represents the output vector, y represents the real label.

Additionally, the Accuracy Score (see Eq.16) is also adopted as another important metric to evaluate the training performance, which reflects the proportion of correct predictions out of the total number of samples. Among the items in Accuracy equation, TP (true positive) means that the prediction is positive, and the actual label is also positive. TN (true negative) means that the prediction is negative, and the actual label is also negative. FP (false positive) means that the prediction is positive, while the actual label is negative. FN (false negative) means that the prediction is negative, while the actual label is positive.

Fig. 12 shows the training process of the ResNet model for recognizing structure type (Fig. 12b), roof material (Fig. 12c), and wall material (Fig. 12d). The initial learning rate and training epochs are set as 0.001 and 200 according to preliminary trials. The training efficiency is high at the beginning stage, while no significant improvement (the decay of loss function and accuracy) can be observed after 50 epochs, indicating that the model has almost converged. Finally, the loss value converges to around 0.1 for both the structure type, roof material, and wall material, and the accuracy value converges to around 0.93 for the three classification items. The overall loss also converges to 0.3 and overall accuracy converges to 0.94, which indicates that the model performs well on the training dataset.

After training, the well-trained model was evaluated on the testing dataset containing a total of 932 images. The Accuracy, Recall, Preci-

Table 6
Indicators of the model performance for structure attribute recognition in the testing dataset.

Item	Overall accuracy	Precision	Recall	F1-score
Structure type	0.70	0.70	0.70	0.70
Roof material	0.76	0.74	0.76	0.74
Wall material	0.75	0.74	0.75	0.74

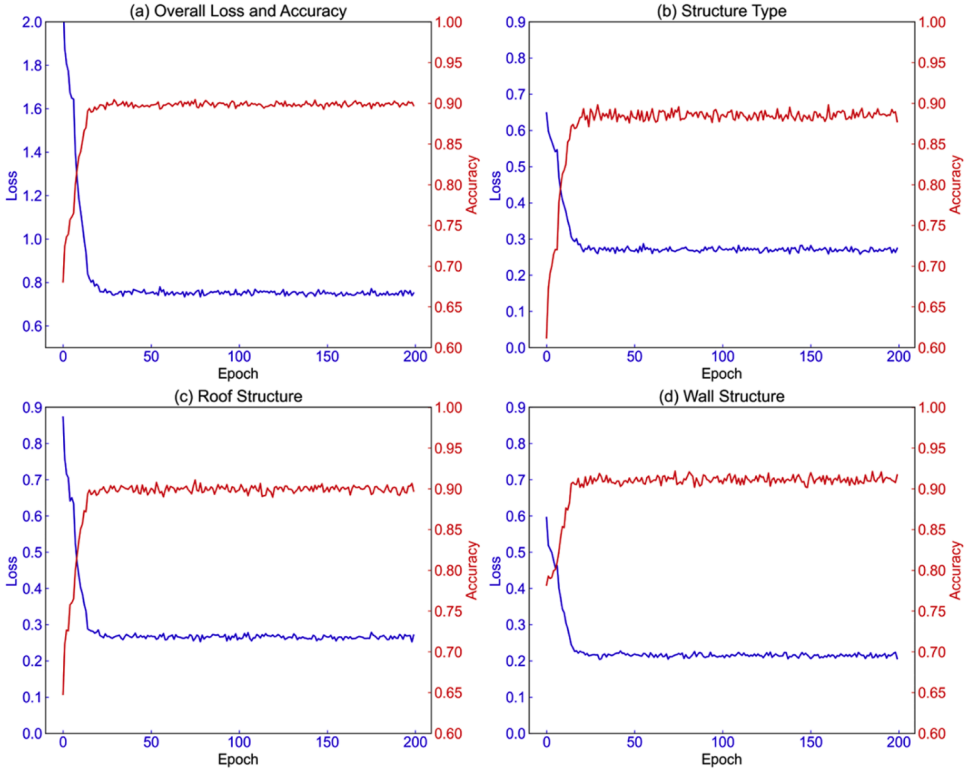

Fig. 12. Training process of our ResNet model for structural attribute recognition.

sion, and F1-score (formulated as Eqs.16-19) were used as the evaluation metrics, and the testing results are shown in Table 6. Among the three categories, the model performs best in recognizing roof material, with an overall accuracy of 0.76 and a balanced recall and F1-score of 0.76 and 0.74, respectively. Wall material recognition follows closely, achieving a 0.75 accuracy and similarly balanced precision and recall (both 0.74–0.75), indicating strong and consistent performance. In contrast, structure type recognition yields slightly lower scores across all metrics (0.70), possibly due to higher intra-class variability or visual ambiguity in the data. Across all tasks, the near-equal values of precision and recall indicate the model maintains a good balance between false positives and false negatives. The consistent F1-scores further support the model's robustness across categories. Overall, the results suggest the model is reliable for structural attribute classification, particularly for roof and wall materials, while improvements may be needed for better structure type identification.

$$Accuracy = \frac{TP + TN}{TP + TN + FP + FN} \tag{16}$$

$$Precision = \frac{TP}{TP + FP} \tag{17}$$

$$Recall = \frac{TP}{TP + FN} \tag{18}$$

$$F1 = 2 \cdot \frac{Precision \cdot Recall}{Precision + Recall} \tag{19}$$

Some classification examples from the testing dataset are shown in Fig. 13, which highlights potential cases of misclassification. For instance, tree occlusion and shadows (Fig. 13a) can partially block the façade, making it difficult to reliably identify wall materials or structure height. In addition, visual similarities between certain materials (e.g., light-colored wood siding versus painted brick, or asphalt shingles versus dark tiles) may cause confusion, shown as Fig. 13b. Additionally, small construction details can be misinterpreted under different lighting or resolution. Overall, the challenges posed by occlusion, texture similarity, and image quality are the main factors of misclassifications, remaining to be solved in future work.

Demonstration for the 2025 Eaton fire

The Eaton Fire was a devastating wildfire that broke out in Los Angeles County, Southern California, in January 2025. The perimeter of the study region of the Eaton fire is shown in Fig. 3, covering 14021 acres (56.74 km^2). The coordinates of the fire center are 34.205°N, 118.088°W. It ignited on the evening of January 7, 2025, in Eaton Canyon within the San Gabriel Mountains. Driven by intense Santa Ana winds, the fire rapidly spread into nearby foothill communities, with Altadena being especially hard hit. The blaze claimed the lives of at least 18 people and destroyed over 9,000 structures, making it the fifth deadliest and second most destructive wildfire in California's history. After burning for 24 days, the fire was fully contained on January 31.

After retrieving and filtering house images based on the input addresses in the area impacted by the Eaton fire, a total of 3,951 house images were collected. These images were processed using the proposed structural attribute recognition method and fuel load calculation model to estimate the structural fuel load for each building. In this section, we compare the estimated fuel load data in the area impacted by the Eaton fire derived from structure attributes identified by our AI model, with reference data where structure attributes are obtained from the DINS dataset. It is important to note that the true benchmark of structural fuel load remains unknown. The comparisons presented in this study are based solely on the estimated fuel loads calculated using the same set of physical equations, applied respectively to structural attributes identified by the AI model and those recorded in the DINS database. Therefore, the comparison fundamentally reflects the accuracy of structural attribute recognition, rather than the absolute correctness of the fuel load values.

Fig. 14(a) compares the fuel load estimations based on the structure attribute recognition result from AI against the reference data that the structure attribute information was derived from DINS. Blue points represent individual sample estimates, and the red line represents the ideal 1:1 match between AI and DINS estimation, meaning a perfect agreement. The distribution appears tight along the red line, especially in the mid-value range (100 GJ), suggesting strong overall agreement. The coefficient of determination (R^2) of two groups of fuel load data is 0.95, indicating the methodological consistency and feasibility between the two estimations under the same modeling assumptions. The Root Mean Square Error (RMSE) measures the average magnitude of the estimation error. While this value (23.7 GJ) is relatively high, it is reasonable and expected for a wide data range and high-magnitude fuel loads. Overall, the AI model is suitable for identifying structure attributes, including wall, roof, and dimensions, that are key inputs to fuel load calculation. Combined with physics-based evaluation of fuel load for prototype wall and roof assemblies, the AI model can serve to characterize fuel load in a community.

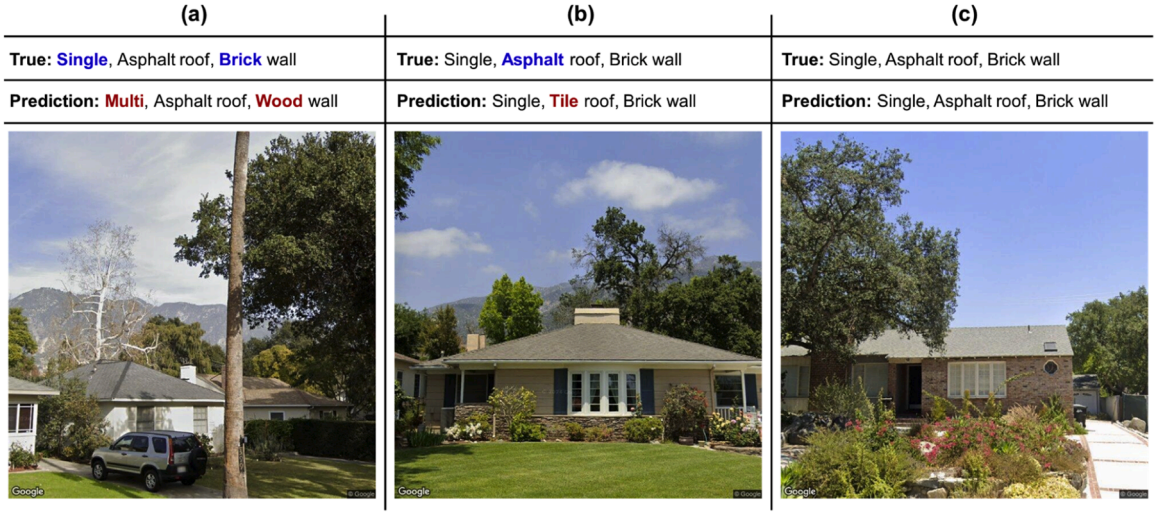

Fig. 13. Some classification examples in the testing dataset. (a) misclassify structure type and wall material, (b) misclassify roof material, (c) totally correct. All images are from Google Map © Google.

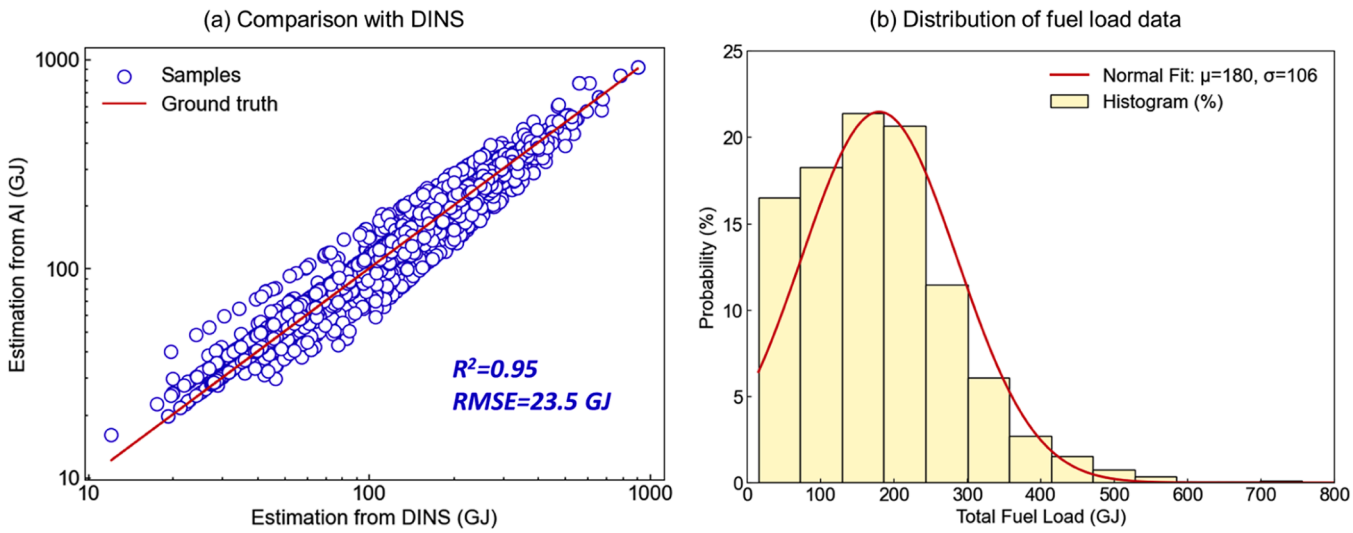

Fig. 14. Fuel load data in the studied area impacted by the Eaton fire estimated from AI and DINS dataset.

Additionally, the estimated fuel load data both from AI and DINS are plotted in the area impacted by the Eaton fire to visualize the fuel load distribution of this area, show as Fig. 15. From the fuel load map, high fuel load areas (>400 GJ) dominate the western edge (Altadena), and a dense band of high fuel loads also stretches eastward along the base of the San Gabriel Mountains. Moreover, extreme fuel loads (>500 GJ) are concentrated near foothill residential zones, indicating the potential for high-intensity combustion in case of a WUI fire. The cosine similarity of two figures derived from AI estimation and reference data in DINS is around 0.98, indicating a high level of agreement under the same modeling assumptions. This comparison visually demonstrates the power and potential divergence of AI-based estimation for structural fuel load mapping in WUI communities, even though it should be interpreted as a measure of consistency rather than a direct validation against independent ground truth. The AI-based fuel load estimation and mapping enable detecting high fuel areas along complex terrain edges, which is crucial for prioritizing ignition-resistant construction and lowering the risk of ignition.

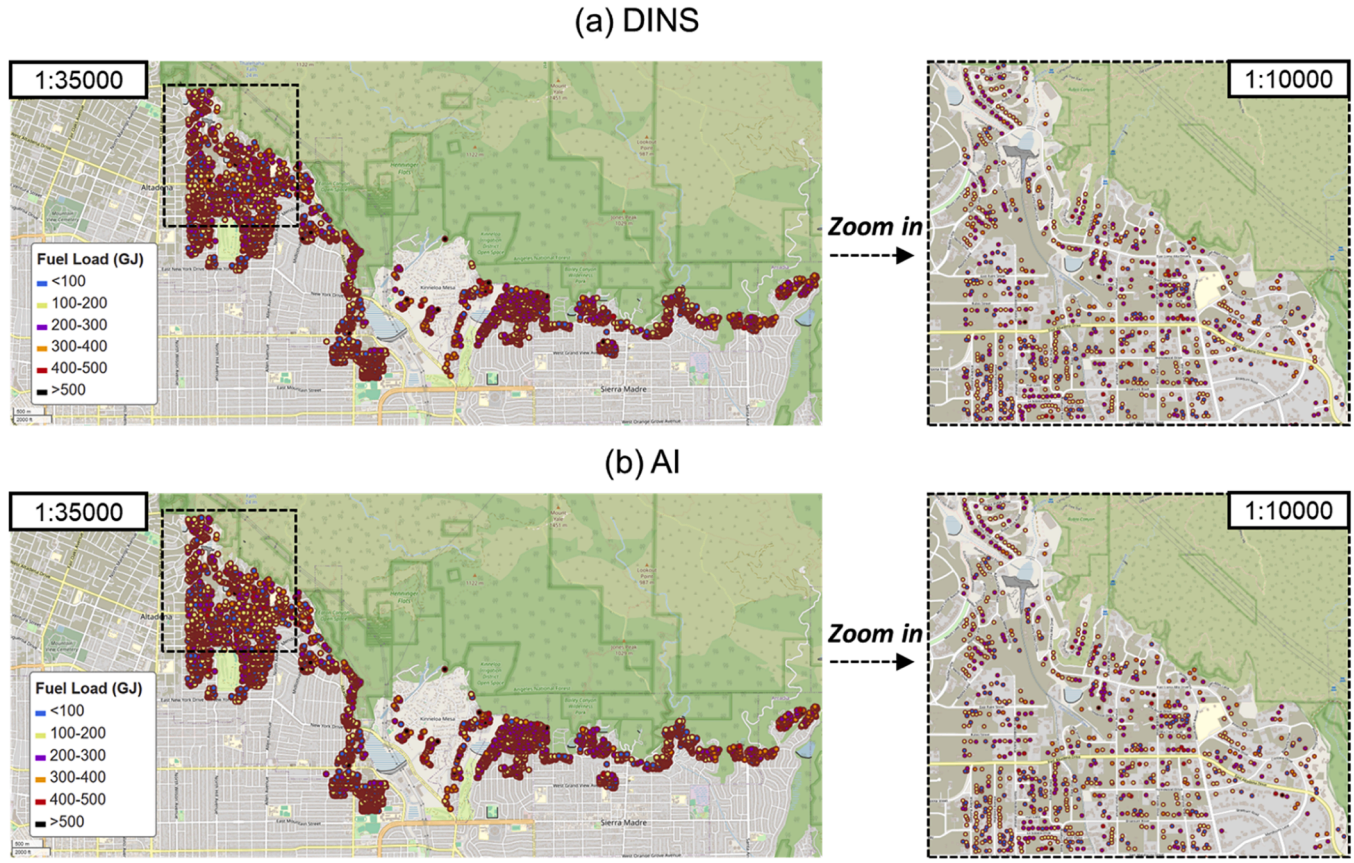

Fig. 15. Fuel load mapping of (a) reference data from DINS, and (b) AI estimation data.

Statistical analysis of estimated fuel load data

Fig. 14(b) displays the distribution of total fuel load measurements as a histogram with a fitted normal distribution curve. Most of the observations cluster between roughly 100 GJ and 300 GJ, peaking around 150 GJ, where the highest probability bin reaches just over 20 %. Beyond 300 GJ the frequency of observations declines sharply, with a long positive tail extending out past 600 GJ, indicating that very high fuel loads are relatively rare in the Eaton area. The fitting results by normal distribution show that the mean (μ) is 174 GJ with a standard deviation (σ) of 101 GJ. From a fire safety management perspective, the concentration of moderate fuel loads implies that many areas pose a typical baseline hazard level, while the relatively few regions with exceptionally high loads, as evidenced by the long tail, could represent critical hotspots requiring prioritized mitigation.

Fig. 16 further shows the fuel load probability distribution across different structure combinations, where all feature non-combustible roof shingles and vary by wall material (combustible vs. non-combustible) and structure type (single-story vs. multi-story) according to the AI recognition results. The result of the combination of non-combustible roof, non-combustible wall, and multi-story structures is shown as Fig. 16(a), where the mean value is around 174 GJ with a standard deviation of 106 GJ. The probability distribution is concentrated at lower values with a steep drop-off, suggesting limited accumulation in such low-hazard constructions. The result of combining non-combustible roof, non-combustible wall, and single-story is shown as Fig. 16(b), where the mean value is around 178 GJ with a standard deviation of 101GJ. Compared with combination (a), its mean value is unexpectedly slightly higher. This could be attributed to the larger footprint of the single-story configuration in combination (b), which leads to a disproportionately high roof fuel load that outweighs the reduction in wall fuel load compared to combination (a).

The result of combining non-combustible roof, combustible wall, and multi-story is shown as Fig. 16(c), where the mean value is around 244 GJ with a standard deviation of 136 GJ. This category shows a higher mean value and wider spread compared to combining (a) and (b). The distribution is still right-skewed but more dispersed, with a notable portion of data above 400 GJ. The result of combination of non-combustible roof, combustible wall, and single-story structures is shown as Fig. 16(d), where the mean value is around 217 GJ with the standard deviation of 109 GJ, which is intermediate between combination (b) and (c). This group also shows a broad peak and long tail, indicating more variability. The fuel load is higher than in fully non-combustible structures, but less than the multi-story combustible-wall structure. Overall, these results demonstrate that while fuel load generally scales with building height, the use of combustible wall materials remains a more dominant factor in increasing total mass and the higher fuel load observed in single-story structures with non-combustible walls suggests that an expanded building footprint can occasionally result in a higher energy potential due to a disproportionately large roof contribution.

Although the roof shingles in the case study are non-combustible, the internal composite materials and wooden trusses are flammable and contribute substantially to the total structural fuel load. The comparison of wall fuel load and roof fuel load for different structure combinations is shown in Fig. 17. In all cases, roof fuel load is significantly greater than wall fuel load, particularly in combinations (a) and (b). Combination (a) with a multi-story structure has a higher wall fuel load than the single-story combination (b). However, the roof fuel load in (b) exceeds that in (a), resulting in a higher overall fuel load. In short, for structures with non-combustible walls, the total fuel load of a single-story building may exceed that of a multi-story building due to the larger contribution from roof components and larger footprint area. In contrast, for structures with combustible wall shingle (combination c-d), the wall contributes a larger proportion of the total fuel load. Compared to combinations (a) and (b), there is a more noticeable trend of increasing total fuel load

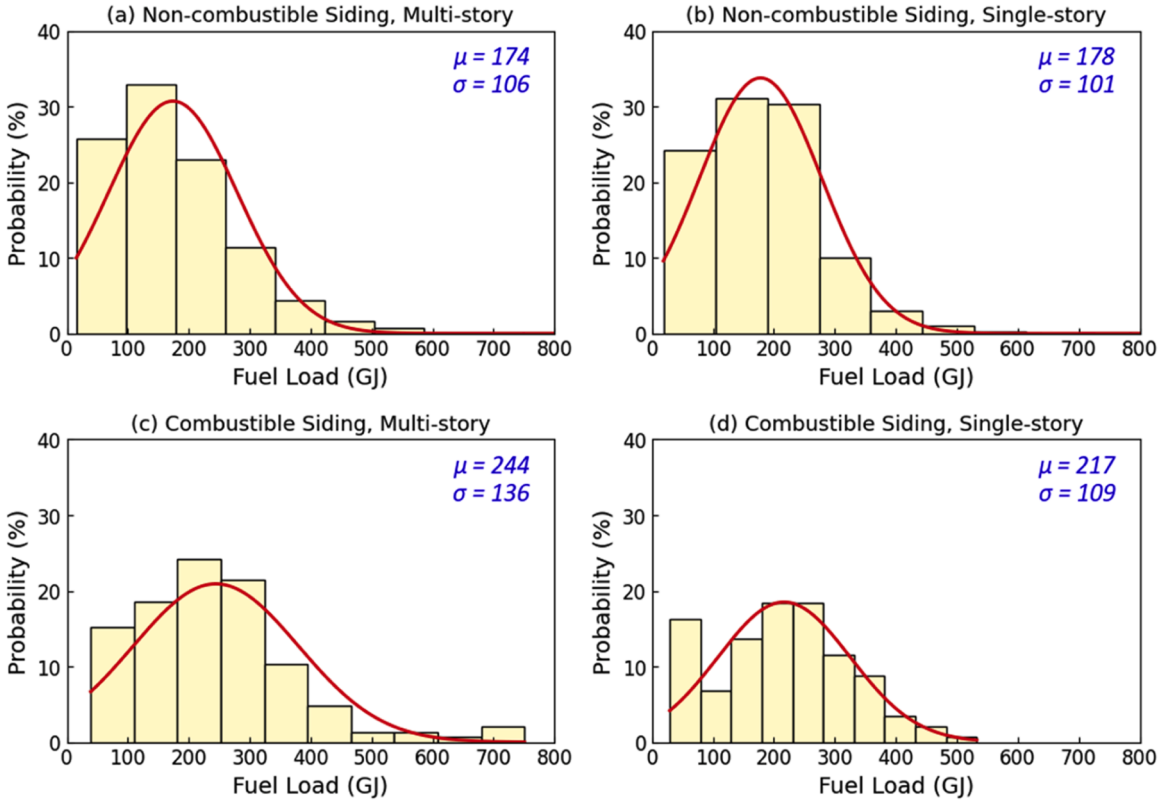

Fig. 16. Comparison of fuel load distributions of different structure combinations with non-combustible roof, (a) non-combustible wall siding with multi-story, (b) Non-combustible wall siding with single-story, (c) combustible wall siding with multi-story, (d) Non-combustible wall siding with single-story.

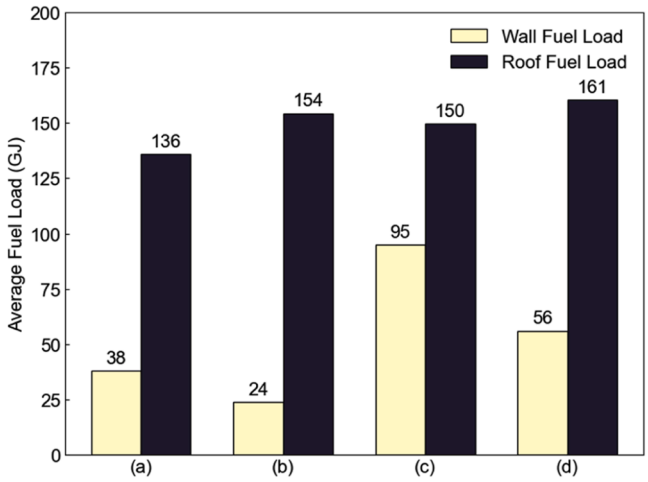

Fig. 17. Comparison of roof fuel load and wall fuel load for different structure combinations.

with building height.

Discussion

Fire duration estimation from structural fuel load

This section provides a conceptual discussion of how the estimated structural fuel load could be coupled into fire spread modelling. To translate the estimated structural fuel load into a functional parameter for fire spread modelling, it is necessary to establish their relationships. As discussed in the introduction, the structural fuel load defines the total energy available, which directly determines the maximum of total fire duration or combustion time of a structure based on energy consideration. In principle, the total fire heat release (or fuel load) can be formulated as,

$$Q = \int HRR\ dt_1 + \int HRR\ dt_2 + \int HRR\ dt_3 \tag{20}$$

where, t_1, t_2, t_3 respectively represent the durations of growth stage, fully developed stage, and decay stage. There are four unknowns in this equation. Therefore, it is required to make some reasonable assumptions, for example, assigning constant values to the peak HRR, t_1, and t_3 based on the assumptions and calibrations from the experimental data reported in the literature to estimate the total fire duration. Such calibration is not performed in the present study. Therefore, rather than providing a direct estimation of fire duration, this formulation is presented here to conceptually illustrate how SFL could be linked to fire development characteristics.

In the WUI fire spread modelling, the fire duration not only directly determines the active burning time of a structure cell, but it also affects the fire brand generations in some WUI fire spread simulations, which serve as the primary mechanism of heat transfer and ignition. Therefore, the structural fuel load can be used as a dynamic parameter to estimate the burning time to further adjust the quantity and time of the fire brand generation, thereby refining the estimation structural ignition and combustion process in the WUI fire simulations for structure-to-structure or structure-to-vegetation fire spread. Preliminary work on the influence of SFL on fire spread has been explored in our another study [25], which provides initial support for the concept discussed here.

Damage degree forecast from structural fuel load

Structural fuel load will influence fire spread and eventually the degree of damage to the built environment in the WUI. The ignition probability of structures will be influenced by the amount of radiant heat and embers generated by the burning of surrounding structures, which directly depend on their fuel load. Prediction of fire spread is complex as the mechanism is influenced by many factors, including but not limited to the angle and area of the eaves, structure fire resistance, and the surrounding environmental factors such as the proportion of vegetation cover and the distances among the structures. Therefore, the prediction of the structural damage degree after fire is a multifactorial problem that extends beyond fuel load alone. Nevertheless, fuel load is a key input parameter to enable the prediction of fire spread and resulting damage [25].

The DINS dataset records millions of structure damage data due to wildfires, containing structure construction attributes and geographic locations, which is a valuable resource for investigating the causes of structural fire damage. In future work, we can utilize machine learning methods to develop a non-linear model capturing the relationship between structural damage and multiple contributing factors, including fuel load. Additionally, machine learning methods can also be used to analyze the independence and sensitivity of each factor, offering deeper insights into the interactions between structural characteristics and fire behaviors in WUI.

Case of sensitivity analysis for structural model assumptions

To further quantify the impact of simplified modeling assumptions, a preliminary sensitivity analysis was conducted on a representative residential structure in Eaton area, California with a footprint of 4.7m × 14.1m and the wall height of 3.23m. The construction material of roof is asphalt, and the exterior walls are composed of stucco-brick-cement-based materials. Several variations were introduced, including (1) using alternative roof geometry (open gable roof), (2) inclusion of a wooden deck (3.0m × 3.6m × 0.038m, cedar with wood stud support), and (3) the use of actual wall height instead of simplified classification.

The results shown in Table 7, compared to the prototype model, the open gable roof results in a minor increase in SFL (0.75%), while incorporating a wooden deck leads to a more noticeable increase (5.08%) due to the additional combustible material. In contrast, using the actual structural height reduces the estimated SFL by 3.69%, reflecting differences in dimension assumption.

These results indicate that simplified assumptions can introduce variations on the order of a few percent in SFL estimates, depending on the specific structural features considered. In particular, secondary combustible components such as decks may have a more significant impact, while geometric simplifications (e.g., roof type) tend to produce smaller deviations. Therefore, the SFL estimates presented in this study should be interpreted as approximate values under simplified assumptions rather than precise quantifications. Overall, the observed variations are relatively small. Therefore, considering the current limited precision of AI-based structural attribute recognition, simplified prototype assumptions provide a reasonable approximation, although further refinement would be beneficial in future studies.

Assumptions and limitations

In this study, several assumptions were introduced to simplify the

Table 7
Sensitivity analysis of SFL estimations to key structural assumptions for a structure case.

Model No.	Attribute variable	Fuel load (MJ)	Variation (%)
0	Prototype	47,383	/
1	Open gable roof	47,741	0.75
2	With deck	49,791	5.08
3	Using real height	45,636	-3.69

structural modeling and fuel load estimation processes. For instance, we assumed that all structures share a uniform geometric configuration and roof style. Structural height was also approximated using a binary classification of single or multi-story buildings. This work neglects some details of the secondary combustible components such as decks, fences, and underlayment, which are critical to initial ignition pathways. These simplifications of prototype model can cause inevitable errors and variations of fuel load assessment compared to reality. Additionally, construction materials were derived from the DINS dataset, although this dataset does not capture the full diversity of materials used in real-world construction. These simplifications inevitably overlook various structural attributes and may lead to approximations in the estimation of fuel load. Such assumptions are made considering the current limitations in obtaining high-precision geometric measurements and detailed structural attribute identifications. The essential parametric analysis and sensitivity analysis would be conducted to quantify the uncertainties of these assumptions proposed in the future work, which remains a challenge currently due to the limited availability of comprehensive experimental benchmarks. A more systematic sensitivity analysis, incorporating detailed structural representations and controlled comparisons, is an important direction for future research. Nonetheless, they significantly reduce the complexity and effort involved in data collection and fuel load calculations, while still maintaining a reasonable level of accuracy and reliability. When higher-resolution geospatial data and more granular LiDAR-derived building details become accessible, the geometric inputs can be refined without altering the core fuel-load calculation logic.

In terms of limitations, beyond those introduced by the underlying assumptions, the validation of the estimation method remains relatively coarse and is constrained by insufficient experimental data support. Due to the limited availability of full-scale fire experiments involving entire houses, there is no established statistical conclusion regarding the total energy released after the complete combustion of a structure, which causes difficulties in our method comparison validation. Additionally, the performance of the AI model in recognizing structural attributes is suboptimal. This limitation arises not only from the model's constrained feature extraction capabilities, but also from the low visual variance among different construction materials. The SFL calculation depends primarily on the assigned material type and associated thermophysical properties. Therefore, the effect of misclassification varies depending on the similarity between material classes. For example, confusion between non-combustible (e.g., metal and brick) results in relatively small deviations in SFL, due to their limited heat of combustion. In contrast, misclassification involving combustible materials (e.g., wood) may introduce larger variations, as these materials contribute more significantly to fuel load. In addition, roof and wall materials contribute differently to the total SFL depending on their relative surface areas, implying that errors in dominant structural components have a greater influence on final estimates. The observations in Section 5.2 suggest that the impact of recognition errors is uneven across individual structures and is moderated at the community level. Analysis of the confusion matrices (shown as Fig. A1 in Appendix) derived from the independent testing dataset further indicates that the majority of misclassification cases occur among material classes with relatively similar combustible characteristics. For example, in roof-material classification, the most frequent confusion occurred between tile and asphalt roofs, with 744 tile-roof samples misclassified as asphalt roofs. Although this reduced the classification accuracy, the corresponding SFL deviation remained comparatively limited because both roof types exhibit relatively similar combustible characteristics. In contrast, wall-material misclassification involving wood and stucco/brick/cement classes may produce substantially larger SFL deviations because of the significantly different heat-release contributions associated with combustible wood materials. Specifically, 764 wood-wall samples were classified as stucco/brick/cement walls in the testing dataset. However, these high-impact combustible classes account for a relatively small proportion of the total building inventory. Therefore, the impact of recognition errors on the final community-scale SFL estimation is influenced by both the structure attribute differences between the true and predicted classes and the relative frequency of these classes in the study area. Therefore, the reported agreement reflects a combined effect of multiple material categories rather than being dominated by a single classification. Nonetheless, it is necessary to adapt more advanced and fine-grained feature perception techniques and more intelligent material identification strategies to improve the recognition accuracy of structure attributes.

In addition, it should also be noted that vinyl siding was not explicitly treated as a direct combustible fuel component in the present SFL calculation framework. This treatment represents a modeling simplification rather than an assumption of non-combustibility. Under sufficient thermal exposure, particularly during intense radiant heating or structure-to-structure fire spread, vinyl siding may contribute additional combustible fuel and alter façade burning behavior. Therefore, the current framework may underestimate SFL in certain high-exposure scenarios. This limitation arises primarily from the lack of sufficiently validated full-scale benchmark data and the large variability in vinyl material properties and installation conditions. Future work will incorporate more detailed façade material characterization and sensitivity analyses to better quantify the contribution of secondary combustible exterior components.

Conclusions

This study presents a novel AI-driven framework for assessing structural fuel load in Wildland-Urban Interface (WUI) communities, addressing a critical data gap in fire hazard evaluation. By leveraging deep convolutional neural networks, remote sensing, and open datasets such as the DINS database, the proposed method enables automated identification of external combustible materials, namely wall and roof from existing publicly available street image data and geospatial sources. The model provides automated classification of construction materials and structure attributes with moderate accuracy and recognized uncertainty and estimates structure dimensions, which are then used to calculate fuel load based on physical combustion properties. The fuel load calculated by our physical model with the prototype for the same house configuration is compared with the total heat release data of a group of burning tests, resulting in an error of only 4.3%, providing a preliminary consistency check and feasibility of the proposed method. The AI model was trained and validated using real-world fire data from the 2025 Palisades fires, achieving reasonable predictive performance in material and structure type recognition for fuel load estimation, where the overall accuracy of structure attributes exceeds 0.7.

The proposed method is also applied to a case study in the area impacted by the 2025 Eaton fire, which was not used for training, where the AI-based fuel load estimations show reasonable methodological consistency and feasibility (over 95% similarity) with those derived from the DINS database under the same modeling assumptions. The analysis of fuel load distributions in the case study reveals that most structures in the study area exhibit moderate loads with a mean value of 180 GJ. Roofs consistently contribute more fuel load than walls, making single-story non-combustible structures sometimes have higher potential energy release than multi-story structures. Overall, this method supports a refined assessment of fuel load data in communities, which can serve to enhance existing fire spread models.

In future work, this framework can be extended to include more structural elements such as decks, fences, as well as temporal analysis of vegetation growth and maintenance. Efforts should also focus on incorporating indoor content fuel load estimates in addition to structural fuel load. Moreover, integrating fire exposure simulations with the AI-estimated fuel load data will enable more accurate predictions of fire spread results. Additionally, the spatial distribution of structural fuel load data can be validated through comparison with structural damage

level statistics, providing a valuable basis for exploring their correlations. Overall, even though this work is not intended to directly assess fire risk, it provides actionable data to support downstream fire spread modeling and risk analysis for enhancing community resilience.

CRediT authorship contribution statement

Yifei Ding: Writing – original draft, Visualization, Software, Methodology, Funding acquisition, Formal analysis. **Thomas Gernay:** Writing – review & editing, Supervision, Methodology, Formal analysis, Conceptualization. **Xuechun Li:** Writing – review & editing, Formal analysis, Data curation. **Negar Elhami-Khorasani:** Writing – review & editing, Supervision, Methodology, Conceptualization. **Susu Xu:** Writing – review & editing, Formal analysis. **Xinyan Huang:** Writing – review & editing, Supervision, Methodology, Funding acquisition, Conceptualization.

Declaration of competing interest

Dr. Xinyan Huang is a Guest Editor of Applications in Energy and Combustion Science, but he was not involved in the peer-review or decision-making process for this paper. The authors have no other conflicts of interest.

Acknowledgements

XH Thanks the support from National Natural Science Foundation of China (NSFC No. 52322610) and PolyU RISDU Joint Research Fund (JRF No. P0058005). YD thanks the support from the SFPE Foundation Student Research Grant and the PolyU PhD Scholars International Collaborative Research Fellowship (ICRF).

Supplementary materials

Supplementary material associated with this article can be found, in the online version, at doi:10.1016/j.jaecs.2026.100525.

Appendix

Fig. A1.

Algorithm 1
2D oriented minimum bounding box algorithm.

```
Input: Footprint with irregular shape
Output: Width and length of footprint bounding box
# Step 1: Compute the convex hull of the points
hull ← convexHull (points)
min_area ←∞
best_box ← None
# Step 2: Loop through each edge of the convex hull
for each edge (p1, p2) in hull do
angle ← atan2(p2.y - p1.y, p2.x - p1.x)
rotated ← rotate (points, -angle)
min_x, max_x ← minMax (rotated.x)
min_y, max_y ← minMax (rotated.y)
area ← (max_x - min_x) * (max_y - min_y)
# Step 3: Track the minimal area
if area < min_area do
min_area ← area
width ← max_x - min_x
length ← max_y - min_y
end for
return width, length
```

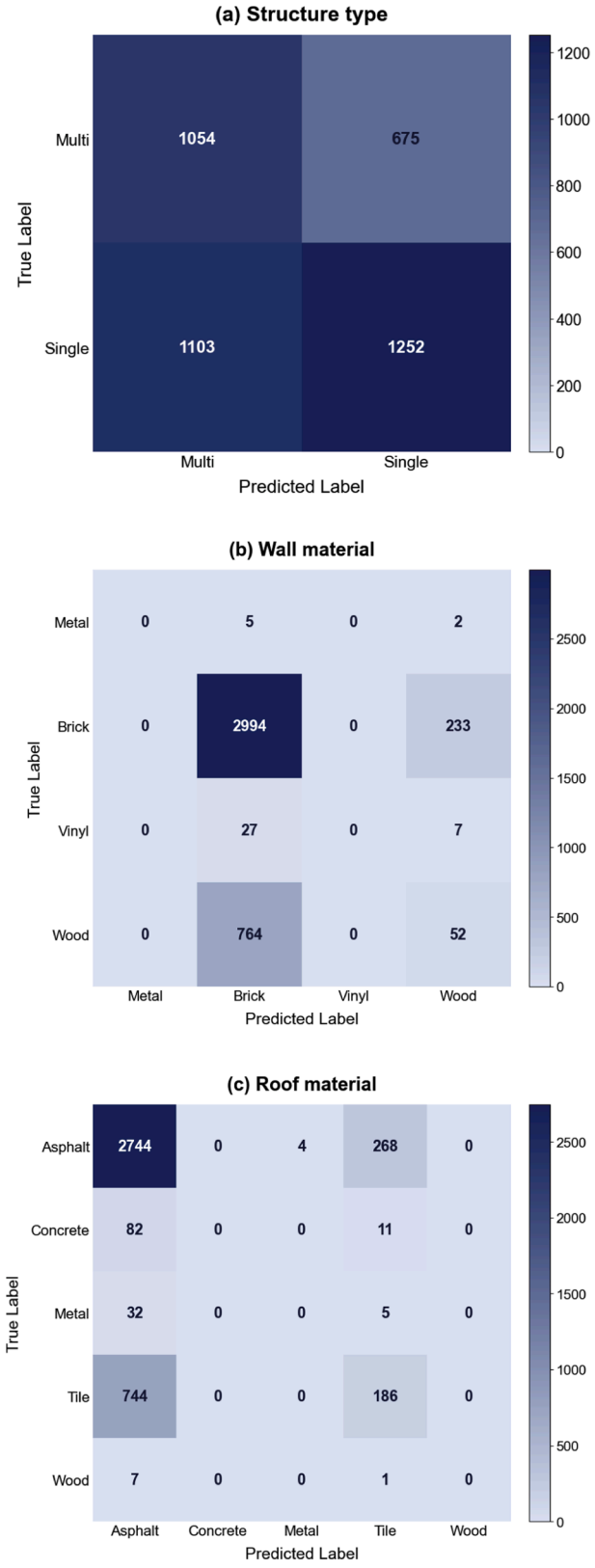

Fig. A1. Confusion matrices of AI structure attribute classification results from the testing dataset.

Data availability

Data will be made available on request.

References

[1] National Interagency Coordination Center. National interagency coordination center wildland fire summary and statistics annual report. https://www.nifc.gov/nicc/; 2006.

[2] National Interagency Coordination Center. National interagency coordination center wildland fire summary and statistics annual report 2024. https://www.nifc.gov/sites/default/files/NICC/2-Predictive%20Services/Intelligence/Annual%20Reports/2024/annual_report_2024.pdf.

[3] Kim Y, Cho Y, Heo HK, Lim L. Estimating casualties from urban fires: a focus on building and urban environment information. Sustain Cities Soc 2024;115:105839. https://doi.org/10.1016/j.scs.2024.105839.

[4] National Interagency Coordination Center, Wildland fire summary and statistics annual report 2024, 2025. chrome-extension://efaidnbmnnnibpcajpcglclefindmkaj/nifc.gov/sites/default/files/NICC/2-Predictive Services/Intelligence/Annual Reports/2024/annual_report_2024.pdf.

[5] Qiu M, Chen D, Kelp M, Li J, Huang G, Yazdi MD. The rising threats of wildland-urban interface fires in the era of climate change: the Los Angeles 2025 fires. Innov 2025.

[6] Szasdi-Bardales F, Shamsaei K, Juliano TW, Kosovic B, Ebrahimian H, Elhami-Khorasani N. An offline coupling of fire spread models to simulate the 2021 Marshall Fire. Int J Wildl Fire 2025;34.

[7] Filkov AI, Tihay-Felicelli V, Masoudvaziri N, Rush D, Valencia A, Wang Y, Blunck DL, Valero MM, Kempna K, Smolka J, De Beer J, Campbell-Lochrie Z, Centeno FR, Ibrahim MA, Lemmertz CK, Tam WC. A review of thermal exposure and fire spread mechanisms in large outdoor fires and the built environment. Fire Saf J 2023;140:103871. https://doi.org/10.1016/j.firesaf.2023.103871.

[8] Elhami-Khorasani N, Ebrahimian H, Buja L, Cutter SL, Kosovic B, Lareau N, Meacham BJ, Rowell E, Taciroglu E, Thompson MP. Conceptualizing a probabilistic risk and loss assessment framework for wildfires. Nat Hazards 2022;114:1153–69.

[9] Lin S, Cui W, Wang S, Qin Y, Chen Y, Zhang Y, Huang X, Quarles SL, Gollner MJ. Susceptibility to ignition of landscaping mulches exposed to firebrand piles or radiation. Fire Saf J 2025;154:104388. https://doi.org/10.1016/j.firesaf.2025.104388.

[10] Fiorini C, Craveiro HD, Santiago A, Laím L, da Silva LS. Parametric evaluation of heat transfer mechanisms in a WUI fire scenario. Int J Wildl Fire 2023;32:1600–18.

[11] Caton SE, Hakes RSP, Gorham DJ, Zhou A, Gollner MJ. Review of pathways for building fire spread in the wildland urban interface Part I: exposure conditions. Fire Technol 2017;53:429–73. https://doi.org/10.1007/s10694-016-0589-z.

[12] Suzuki S, Manzello SL. Role of accumulation for ignition of fuel beds by firebrands. Appl Energy Combust Sci 2020:100002. https://doi.org/10.1016/j.jaecs.2020.100002. 1–4.

[13] Blanchi R, Leonard JE, Leicester RH. Lessons learnt from post-bushfire surveys at the urban interface in Australia. For Ecol Manage 2006;234:S139.

[14] Mell WE, Manzello SL, Maranghides A, Butry D, Rehm RG. The wildland–urban interface fire problem–current approaches and research needs. Int J Wildl Fire 2010;19:238–51.

[15] Westhaver A. Why some homes survived: Learning from the Fort McMurray wildland/urban interface fire disaster. Toronto, ON, Canada: Institute for Catastrophic Loss Reduction; 2017.

[16] Dossi S, Messerschmidt B, Ribeiro LM, Almeida M, Rein G. Relationships between building features and wildfire damage in California, USA and Pedrógão Grande, Portugal. Int J Wildl Fire 2022;32:296–312. https://doi.org/10.1071/wf22095.

[17] Maranghides A, Mell W. A case study of a community affected by the Witch and Guejito wildland fires. Fire Technol 2011;47:379–420.

[18] Sun X, Brown MA, Cox M, Jackson R. Mandating better buildings: a global review of building codes and prospects for improvement in the United States. Wiley Interdiscip Rev Energy Environ 2016;5:188–215.

[19] Leon R, Rossberg J. Evolution and future of building codes in the USA. Struct Eng Int 2012;22:265–9.

[20] Shih S-Y, Sher W, Giggins H. Assessment of the building code of Australia to inform the development of BIM-enabled code checking system. In: Proc. 19th World Build. Congr. Constr. Soc. 5-9 May; 2013. p. 1–12.

[21] Syphard AD, Brennan TJ, Keeley JE. The importance of building construction materials relative to other factors affecting structure survival during wildfire. Int J Disaster Risk Reduct 2017;21:140–7. https://doi.org/10.1016/j.ijdrr.2016.11.011.

[22] Tong Q, Gernay T. Mapping wildfire ignition probability and predictor sensitivity with ensemble-based machine learning. Springer Netherlands; 2023. https://doi.org/10.1007/s11069-023-06172-x.

[23] Ding Y, Cheung WK, Zhang Y, Huang X. Digitized fuel load survey in commercial and university office buildings for fire safety assessment. Fire Saf J 2024:104287. https://doi.org/10.1016/j.firesaf.2024.104287.

[24] Elhami-Khorasani N, Salado Castillo JG, Saula E, Josephs T, Nurlybekova G, Gernay T. Application of a digitized fuel load surveying methodology to office buildings. Fire Technol 2021;57:101–22.

[25] Ding Y, Saharan N, Elhami-Khorasani N, Gernay T, Zhang Y, Huang X. Coupling computer-vision house fuel load estimation with fire spread simulation in the Wildland–Urban interface. Fire Saf J 2026;162:104713. https://doi.org/10.1016/j.firesaf.2026.104713.

[26] Purnomo DMJ, Qin Y, Theodori M, Zamanialaei M, Lautenberger C, Trouvé A, Gollner M. Reconstructing modes of destruction in wildland–urban interface fires using a semi-physical level-set model. Proc Combust Inst 2024;40:105755. https://doi.org/10.1016/j.proci.2024.105755.

[27] Qin Y, Purnomo DMJ, Theodori M, Zamanialaei M, Lautenberger C, Gollner M, Trouvé A. Simulations of firebrand-driven fire spread in landscape scale Wildland-Urban-Interface (WUI) and urban conflagration models. Fire Saf. J. 2026;162:104686. https://doi.org/10.1016/j.firesaf.2026.104686.

[28] Masoudvaziri N, Szasdi Bardales F, Keskin OK, Sarreshtehdari A, Sun K, Elhami-Khorasani N. Streamlined wildland-urban interface fire tracing (SWUIFT): Modeling wildfire spread in communities. Environ Model Softw 2021;143:105097. https://doi.org/10.1016/j.envsoft.2021.105097.

[29] Hakes RSP, Caton SE, Gorham DJ, Gollner MJ. A review of pathways for building fire spread in the wildland urban interface part ii: response of components and systems and mitigation strategies in the United States. Fire Technol 2017;53:475–515. https://doi.org/10.1007/s10694-016-0601-7.

[30] Suzuki S, Manzello SL. Experimentally producing firebrands showers from disparate fuels to represent the combustion of structural and vegetative fuels simultaneously. Appl Energy Combust Sci 2025;24:100399. https://doi.org/10.1016/j.jaecs.2025.100399.

[31] Lee SW, Davidson RA. Physics-based simulation model of post-earthquake fire spread. J Earthq Eng 2010;14:670–87. https://doi.org/10.1080/13632460903336928.

[32] Standohar-Alfano CD, Estes H, Johnston T, Morrison MJ, Brown-Giammanco TM. Reducing losses from wind-related natural perils: research at the IBHS research center. Front Built Environ 2017;3:1–19. https://doi.org/10.3389/fbuil.2017.00009.

[33] Sharma A, Singh PK, Kumar Y. An integrated fire detection system using IoT and image processing technique for smart cities. Sustain Cities Soc 2020;61:102332. https://doi.org/10.1016/j.scs.2020.102332.

[34] Ding Y, Deng R, Zhang Y, Huang X, Elhami-Khorasani N, Gernay T. Automatic assessment of fuel load and fire risk via digitized database and intelligent computer vision. Process Saf Environ Prot 2025;197:107031. https://doi.org/10.1016/j.psep.2025.107031.

[35] Zhang X, Jiang Y, Wu X, Nan Z, Jiang Y, Shi J, Zhang Y, Huang X, Huang GGQ. AIoT-enabled digital twin system for smart tunnel fire safety management. Dev Built Environ 2024:100381. https://doi.org/10.1016/j.dibe.2024.100381.

[36] Caro J, T Milke. A survey of fuel loads in contemporary office buildings, NIST_GCR-96-697. Gaithersburg, MD: National Institute of Standards and Technology; 1996.

[37] Kumar S, Rao CVSK. Fire loads in office buildings. J Struct Eng 1997;123:365–8.

[38] Bwalya AC, Sultan MA, Bénichou N. A pilot survey of fire loads in Canadian homes, Institute for Research in Construction. National Research Council Canada Ottawa; 2004.

[39] Suzuki S, Brown A, Manzello SL, Suzuki J, Hayashi Y. Firebrands generated from a full-scale structure burning under well-controlled laboratory conditions. Fire Saf J 2014;63:43–51. https://doi.org/10.1016/j.firesaf.2013.11.008.

[40] Himoto K, Shinohara M, Sekizawa A, Takanashi K, Saiki H. A field experiment on fire spread within a group of model houses. Fire Saf J 2018;96:105–14. https://doi.org/10.1016/j.firesaf.2018.01.003.

[41] Yang L, Liu W, Liu Q, Liu S, Tong Y, Xiao Z, Meng T, Wei W, Zhang W. Full-scale Fire Experiment of Timber Buildings in Rural Areas of Southwest China. Int J Archit Herit 2023;17:1505–24. https://doi.org/10.1080/15583058.2022.2043952.

[42] California Department of Forestry and Fire Protection. CAL FIRE Damage Inspection (DINS) Data https://data.ca.gov/dataset/cal-fire-damage-inspection-dins-data.

[43] Buffington T, Scott JG, Ezekoye OA. Combining spatial and sociodemographic regression techniques to predict residential fire counts at the census tract level. Comput Environ Urban Syst 2021;88:101633. https://doi.org/10.1016/j.compenvurbsys.2021.101633.

[44] Moyroud N, Portet F. Introduction to QGIS. QGIS Generic Tools 2018;1:1–17.

[45] Vargas-Munoz JE, Srivastava S, Tuia D, Falcao AX. OpenStreetMap: challenges and opportunities in machine learning and remote sensing. IEEE Geosci Remote Sens Mag 2020;9:184–99.

[46] Rischpater R, Au C. Microsoft mapping: geospatial development with Bing maps and C. Apress; 2013.

[47] Zand M, Etemad A, Greenspan M. Oriented bounding boxes for small and freely rotated objects. IEEE Trans Geosci Remote Sens 2021;60:1–15.

[48] Radford A, Kim JW, Hallacy C, Ramesh A, Goh G, Agarwal S, Sastry G, Askell A, Mishkin P, Clark J. Learning transferable visual models from natural language supervision. Int Conf Mach Learn 2021:8748–63.

[49] Hall DJ, Giglio NM. Architectural graphic standards for residential construction. John Wiley & Sons; 2010.

[50] C. ZONES Building America Best Practices Series 2 https://docs.nlr.gov/docs/fy05osti/38360.pdf.

[51] McKinnon M, Weinschenk C, Dow N, DiDomizio M, Madrzykowski D. Materials and products database (version 1.0.0). Columbia, MD: Fire Saf. Res. Institute, UL Res. Institutes; 2023, 21045. https://materials.fsri.org/.

[52] Fire Characteristics of Rigid Vinyl. https://www.custombuiltpallets.com/wp-content/uploads/2021/10/RPVC_Fire_Reistant_Service_Bulletin_1.pdf; 2021.

[53] NIST Fire Calorimetry Database (FCD) https://doi.org/10.18434/mds2-2314.

[54] Heskestad G. Heat of combustion in spreading wood crib fires with application to ceiling jets. Fire Saf J 2006;41:343–8. https://doi.org/10.1016/j.firesaf.2006.01.008.

[55] He K, Zhang X, Ren S, Sun J. Deep residual learning for image recognition. In: Proc. IEEE Conf. Comput. Vis. Pattern Recognit.; 2016. p. 770–8.

[56] Deng J, Dong W, Socher R, Li L-J, Li K, Fei-Fei L. ImageNet: a large-scale hierarchical image database. In: 2009 IEEE Conf. Comput. Vis. Pattern Recognit; 2009. p. 248–55. https://doi.org/10.1109/CVPR.2009.5206848.
[57] Zhou K, Yang Y, Cavallaro A, Xiang T. Omni-scale feature learning for person re-identification. In: Proc. IEEE/CVF Int. Conf. Comput. Vis.; 2019. p. 3702–12.
[58] Redmon J, Divvala S, Girshick R, Farhadi A. You only look once: unified. Real-time object detection. 2016. http://pjreddie.com/yolo/.
[59] Pei Y, Huang Y, Zou Q, Zhang X, Wang S. Effects of image degradation and degradation removal to CNN-based image classification. IEEE Trans Pattern Anal Mach Intell 2019;43:1239–53.
[60] Mao A, Mohri M, Zhong Y. Cross-entropy loss functions: theoretical analysis and applications. In: Int. Conf. Mach. Learn., PMLR; 2023. p. 23803–28.